NAVAL POSTGRADUATE SCHOOL
MONTEREY, CALIFORNIA

AD-A271 165

‖‖‖‖‖‖‖‖‖‖‖

DTIC
ELECTE
OCT 2 6 1993
S A D

THESIS

EXPERIMENTAL DETERMINATION OF THE SURFACE
DISPLACEMENT OF A SMALL FLEXURAL DISK SONAR
TRANSDUCER FROM SURFACE STRAIN MEASUREMENTS

by

Douglas L. Cuthbert

June 1993

Thesis Advisor: S.R. Baker

Approved for public release; distribution is unlimited

93-25607
‖‖‖‖‖‖‖‖‖‖‖

Experimental Determination Of The Surface Displacement Of A Small Flexural Disk
Sonar Transducer From Surface Strain Measurements

by

Douglas Lee Cuthbert
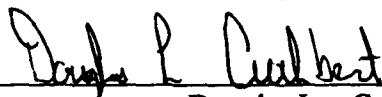Lieutenant, United States Navy
B.S., United States Naval Academy, 1985

Submitted in partial fulfillment of the
requirements for the degrees of

MASTERS OF SCIENCE IN ENGINEERING ACOUSTICS
and
MASTERS OF SCIENCE IN SYSTEMS TECHNOLOGY
(Antisubmarine Warfare)

from the

NAVAL POSTGRADUATE SCHOOL
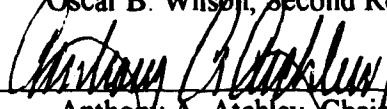June 1993

Author: _____
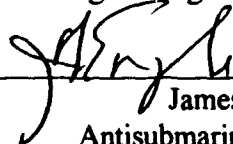Douglas Lee Cuthbert

Approved by: _____
Steven R. Baker, Thesis Advisor

_____
Oscar B. Wilson, Second Reader

_____
Anthony A. Atchley, Chairman
Engineering Acoustics Academic Committee

_____
James N. Eagle, Chairman
Antisubmarine Warfare Academic Group

ABSTRACT

The normal displacement of a flexural disk sonar transducer's radiating face was measured using both a laser doppler vibrometer and surface mounted strain gages. The laser doppler vibrometer measurements were used to calibrate the strain gages, allowing a single measurement of strain to be used to define the displacement over the transducer's entire face. The feasibility of investigating the interaction of closely spaced array elements through the use of surface strain measurements was established by experiments with a submerged two element array. The surface strain, measured as a function of the transducer separation, increases the understanding of sonar transducer element interaction in a densely packed array.

DTIC QUALITY

TABLE OF CONTENTS

ACKNOWLEDGMENT

I would like to acknowledge the following people;

Professors Steve Baker and Bryan Wilson for making this thesis possible. From it's inception they have nurtured it and pushed it along to the final product you see here.

The guys and wives of section IX13 who made this entire journey through academia a fun one, providing me with much camaraderie and leadership.

The U.S. Government and the Navy for giving me the opportunity to spend two years on shore in Monterey, and earn two masters degrees.

My wife Stefani who, as usual, demonstrated super-human support and assistance while having her own thesis and a new baby to contend with.

Finally, Shannon, our beautiful newborn. Though detracting somewhat from thesis time, she had the ability to melt away all the stress of the day with one smile. Thanks Shannon, for putting all of this in perspective for me.

I. INTRODUCTION

A. BACKGROUND

A major thrust in the recent development of active Anti-Submarine Warfare (ASW) detection systems has been the resurgence of interest in active low frequency sonar systems. Despite the revolution in signal processing that has enabled sonar systems to process weak, but useful submarine target signals in the presence of environmental noise, our ability to detect weaker radiated noise has not kept pace with the ever decreasing noise emissions of targets. Thus, our ability to locate and track passively has come into question. Active sonars, not relying on the noise generated by the submarine, are the preferred sensor in the realm of increasingly quiet submarines.

The need for high power, directional low frequency sources has stimulated the research and development of large arrays of flexural mode ("flextensional") transducers. the development of such arrays has led to some interesting problems associated with element-to-element interactions in the case of volumetric arrays of closely-spaced elements, where the nearfield radiation of one transducer is distorted by the presence of another. Though array spacing this close

1

is not the usual case, dense array designs are being considered for some applications.

This thesis describes the development of an experimental technique to measure the vibration of the radiating faces of a pair of small flexural disk sonar transducers, *in situ,* as a function of their separation, using surface mounted strain gages. This project is part of an ongoing research program at the Naval Postgraduate School (NPS) investigating the interaction between sonar transducers in close proximity to one another other, such as in a dense array.

B. OBJECTIVES

The objectives of this research are

(1) Measure the displacement magnitude and phase over the face of two small flexural disk transducers using a laser doppler vibrometer.

(2) Instrument the flexural disk transducers with strain gages and use these gages as displacement indicators by calibrating them, using the laser vibrometer. This technique takes advantage of the strain gage's relatively low cost and ease of application, and its ability to be sensed while submerged and in difficult test situations.

(3) To quantify the interaction between a pair of closely-spaced small flexural disk transducers underwater by measuring the strain in each face for various separation distances.

Small flexural disk transducers were chosen to simplify the measurements and the calculations. Their small size and simplicity of construction greatly eased the handling, testing and theoretical understanding in the experiments.

C. OVERVIEW

This thesis has four major parts. The next chapter discusses the theory of vibrating circular plates, laying the groundwork for the derivation of the normal displacement from the in-plane strain. The third and fourth chapters cover the data taking process. The procedures and results of each experiment will be discussed in its respective chapter before they are brought together for the final calculations and conclusions.

Chapter III describes the direct measurement of the velocity of the transducer's face utilizing a laser doppler vibrometer. Chapter IV describes measurements of the longitudinal strain on the surface of the transducer and how, by using the accurate laser measurements and the strain data, a method of measurement of displacement using the strain gages alone is developed. Finally, Chapter V and six contain the in-water tests, summary, conclusions and recommendations.

II. FLEXURAL DISK TRANSDUCERS

A. GENERAL

Fig. 1 depicts a cross section of a flexural disk sonar
transducer. The theory of flexural disk transducers is
developed by Woollett [Ref. 1]. Flexural disk transducers
are flexural mode resonators which provide good sound
strength and superior electroacoustic efficiency for their
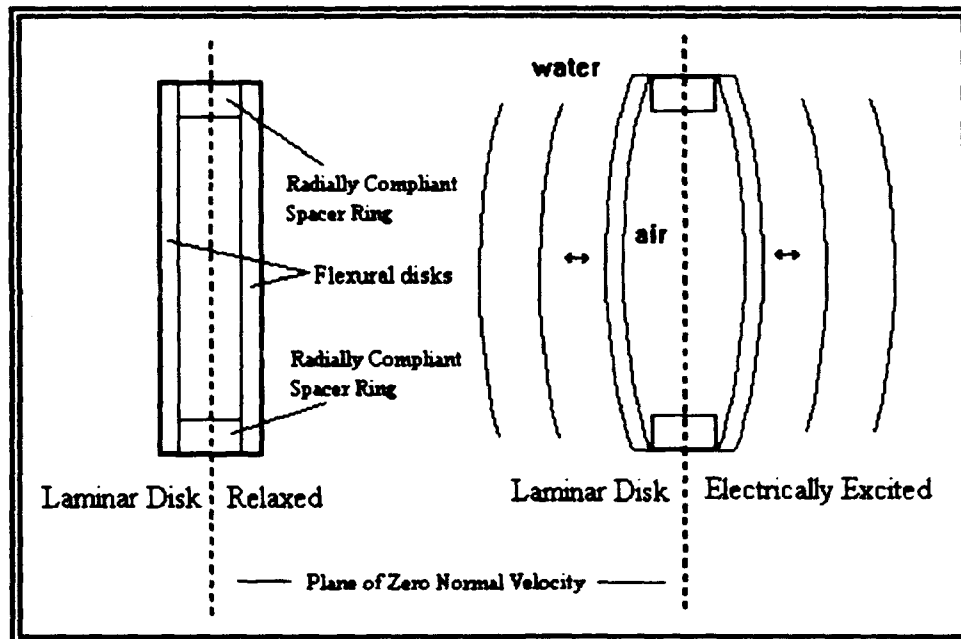

Figure 1   Flexural disk transducer operation.

size. Unlike other types of piezoelectric transducers,
flexural transducers employ the flexure of their shell
rather than the extensional vibrations of the piezoelectric

4

ceramic to radiate sound. Compared to extensionally vibrating resonators, flexural disks have a lower wave velocity and mechanical impedance. This results in a transducer that, for its size, resonates at a lower frequency. These advantages are offset somewhat by the depth limitations imposed on flexural disk transducers, due to the hydrostatic pressure acting on the air-backed vibrating surfaces. The air backing provides a nearly perfect acoustic pressure release on the interior surface of the disk.

Fig. 1 also illustrates the flexural movement of the transducer. The flexural disk transducer studied here consists of two multi-laminar disks in a balanced vibrator with a spacer ring separating them and providing edge support. The small width of the ring minimizes the restraint to rotation at the disk edge. The disks are secured to the spacer with cement and the entire assembly is encased in a waterproof encapsulant. The encapsulant thickness is minimized so as to minimize its effect on the transducer's performance.

The flexural disk transducer is a symmetric vibrator with a velocity node along the plane bisecting the disk. This plane is illustrated in Fig. 1 as a dashed line. Each disk, radiating identically and in phase, act as though it were mounted on an infinite baffle. Only circularly

symmetric vibrations are excited, i.e. only those modes with no nodal diameters.

The transducers tested were tri-laminar flexural disks that use two, Navy type III piezoelectric ceramic disks [Ref. 3] as the flexural bender elements. Each bender element, one on either side of a support ring, is constructed of three layers. The outer layers sandwich the inner piezoelectric ceramic disk. Fig. 2 illustrates the construction of a generic tri-laminar flexural disk. The resonant frequency of interest of our transducers in air is 4100 Hz.
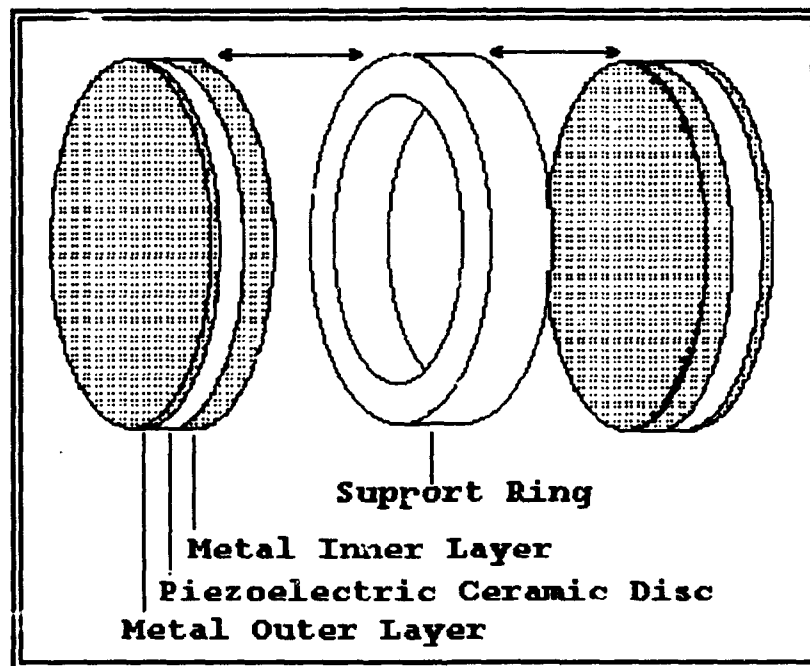
Figure 2 General construction of a tri-laminar flexural disk.

B. NORMAL DISPLACEMENT CURVE

Given idealized boundary conditions for a circular disk, an exact deflection curve for the disk can be calculated using solutions of the difierential equations of motion for the disk. The boundary conditions are dictated by the manner in which the disks are attached to the spacer ring. If the disks are rigidly connected to the ring, allowing no flexure at the edge, then the disk is considered to be clamped (no rotation and no displacement). If the disk lies freely on the ring then it is considered to be simply supported (rotation allowed). It is advantageous to manufacture a flexural disk that is simply supported; clamping the edges would restrict the movement of the disk to the extent that the volumetric displacement and hence the radiated sound would suffer. In practice, actual disks have boundary conditions that are between the extremes of the clamped and the simply supported cases and vary with the construction of each individual transducer. This makes the exact solution by differential equations very difficult.

Woollett [Ref. 1] utilizes an approximate analytical approach toward the calculation of a deflection curve. The approach, using the Rayleigh method, bases the analysis on an assumed polynomial approximation for the deflection. This makes it possible to analyze the disk in terms of algebraic equations that can be manipulated to fit varying

boundary conditions. For the assumed deflection curve, $D(r)$, a power series in polar coordinates is used:

$$D(r) = a_0 + a_1 \frac{r}{A} + a_2 \frac{r^2}{A^2} + a_3 \frac{r^3}{A^3} + a_4 \frac{r^4}{A^4} \qquad (2.1)$$

where

$D(r)$ = normal displacement amplitude of the surface of the disk ,
r = radial coordinate,
A = outside radius of the disk,
$a_0 .. a_4$ = deflection curve coefficients.

Four terms were recommended by Woolett as accurate enough for engineering work, and proved to be suitable for our purposes. Since $\frac{dD}{dr} = 0$ at $r=0$, then a_1 will always be equal to 0. Hence, we assume hereafter a deflection curve of the following form:

$$D(r) = a_0 + a_2 \frac{r^2}{A^2} + a_3 \frac{r^3}{A^3} + a_4 \frac{r^4}{A^4} \qquad (2.2)$$

1. Clamped Edge

The coefficients of the deflection curve for the clamped disk are fairly straightforward to derive. The boundary conditions are that the displacement and the slope vanish at the edge of the disk.

$$D(A) = 0 \qquad (2.3)$$

and

8

$$\left(\frac{dD}{dr}\right)_{r=A} = 0 \qquad\qquad (2.4)$$

For a normalized solution we can set a_0 to one and determine the remaining two coefficients from the boundary conditions. Lamb [Ref. 2] has shown that using a_2 and a_4 and setting a_3 to zero provides good results. From the first boundary condition we have $a_0 + a_2 + a_4 = 0$ Combining this with the information from the second boundary condition, $a_2 + 2a_4 = 0$, we get $a_2 = -2$ and $a_4 = 1$.

2. Simply-Supported Edge

The derivation of the coefficients in equation 2.2 for the simply supported disk is much more complex and only an outline is provided here. The reader can find the complete derivation in [Ref. 1]. The boundary conditions for a simply supported edge are that the normal displacement and the bending stress at the edge both vanish. Three different combinations of coefficients can be derived that satisfy the boundary conditions of the simply supported case. The resulting coefficients depend upon whether or not one of the coefficients is held to zero and, if so, which one. If a_3 or a_4 are held to zero and the remaining coefficients are calculated, the results differ from the case in which no coefficient is held to zero.

9

The results of all three cases are listed in Table 1. The coefficients in the simply-supported case depend upon Poisson's ratio (v); the values listed in Table 1 are

TABLE 1: DEFLECTION CURVE COEFFICIENTS.

	a_0	a_2	a_3	a_4
Clamped	1	-2	0	1
Simply-	1	-1.2453	0	.2453
Supported	1	-1.6047	.6047	0
with $v = 0.3$	1	-1.4417	.3304	.1112

for a Poisson's ratio of 0.3. Fig. 3 illustrates plots of the displacement curves for the coefficient values given. The curves for all three of the simply-supported cases line so close together that only one is shown in Fig. 3. The
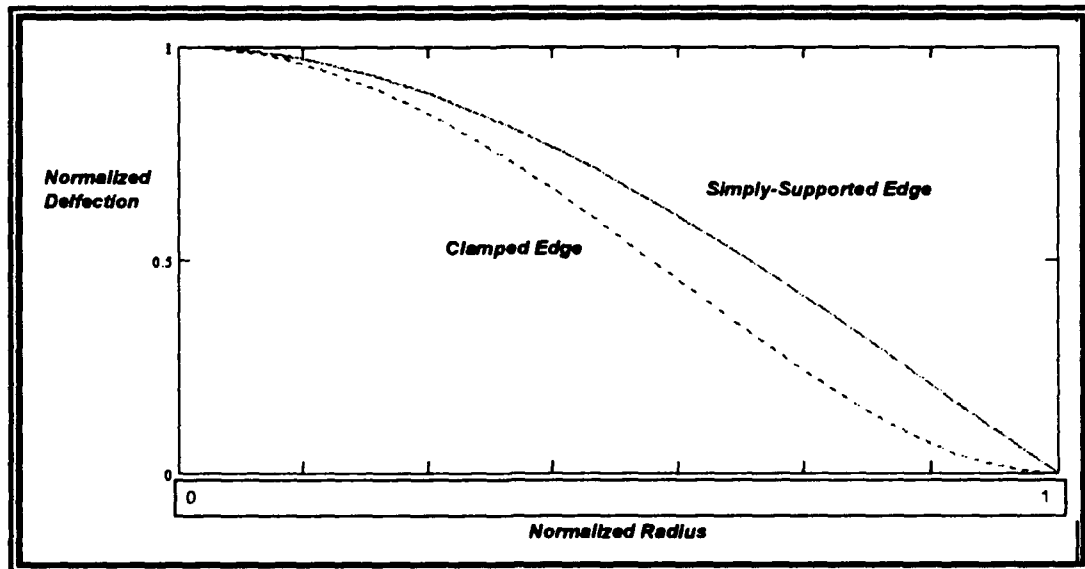

Figure 3 Theoretical deflection curves.

plot for the actual disk is be expected to fall between
these values, as long as only the 0,1 mode is excited.
Experimental verification of this is discussed in Chapter
three.

C. FLEXURAL DISK STRAIN

As each disk deforms, its outside surface is stretched
or compressed in proportion to the local radius of curvature
as depicted in Fig. 4, which shows a cross section of a
circular flexural disk. This results in longitudinal, or
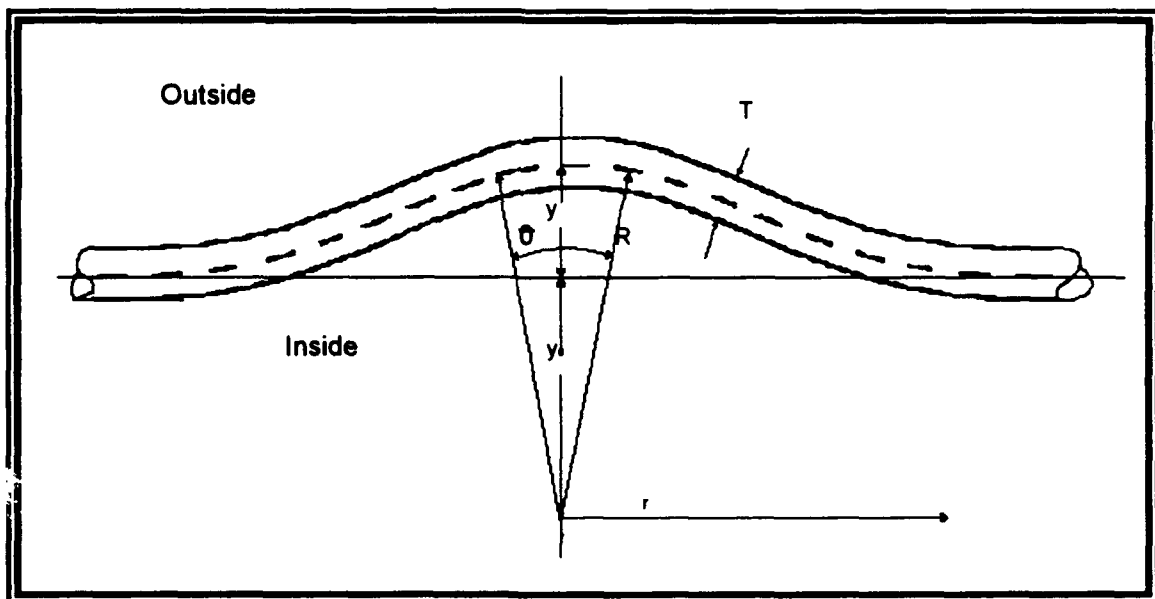

Figure 4 Strain approximation in alexural disk.

tensile, strain in the disk, which we can measure at the
surface with bonded strain gages.   Consider a portion of a
flexural disk approximated by a thin bar of thickness T,

which is displaced a distance y and has a local radius of curvature R, as shown in Fig. 4. Assume a neutral mid-plane where strain is zero (to first order in y.) indicated by the dashed curve in the figure. Refer to Fig 4, the strain on the outside of the transducer face is calculated by,

$$\epsilon = \frac{\text{New length - Old length}}{\text{Old length}} \tag{2.6}$$

$$\epsilon = \frac{(R + \frac{T}{2})\theta - R\theta}{R\theta} = \frac{\frac{T\theta}{2}}{R\theta} = \frac{T}{2R} \tag{2.7}$$

where,

$$(y + y_0)^2 + r^2 = R^2 \tag{2.8}$$

Solving for the radius of curvature,

$$2(y + y_0)dy + 2rdr = 0$$

$$\frac{dy}{dr} = \frac{2r}{2(y + y_0)}$$

$$\frac{d^2y}{dr^2} = \frac{-1}{(y + y_0)} = \frac{-1}{R} \tag{2.9}$$

so the outside strain is,

$$\epsilon = -(\frac{T}{2})(\frac{d^2y}{dr^2}) \tag{2.10}$$

Thus, the strain is proportional to the curvature, or to the second radial derivative of the deflection. By analyzing the curvature for the clamped and simply-supported boundary conditions we can determine the approximate locations of maximum and minimum surface strain that will aide us in

placement of our strain gages for maximum signal.. These
second derivatives are plotted in Fig. 5 for the
displacements shown in Fig. 4. The strain in a simply-
supported disk is maximum at the center and tends to zero at
the edges. As the disk edges become more rigidly held the
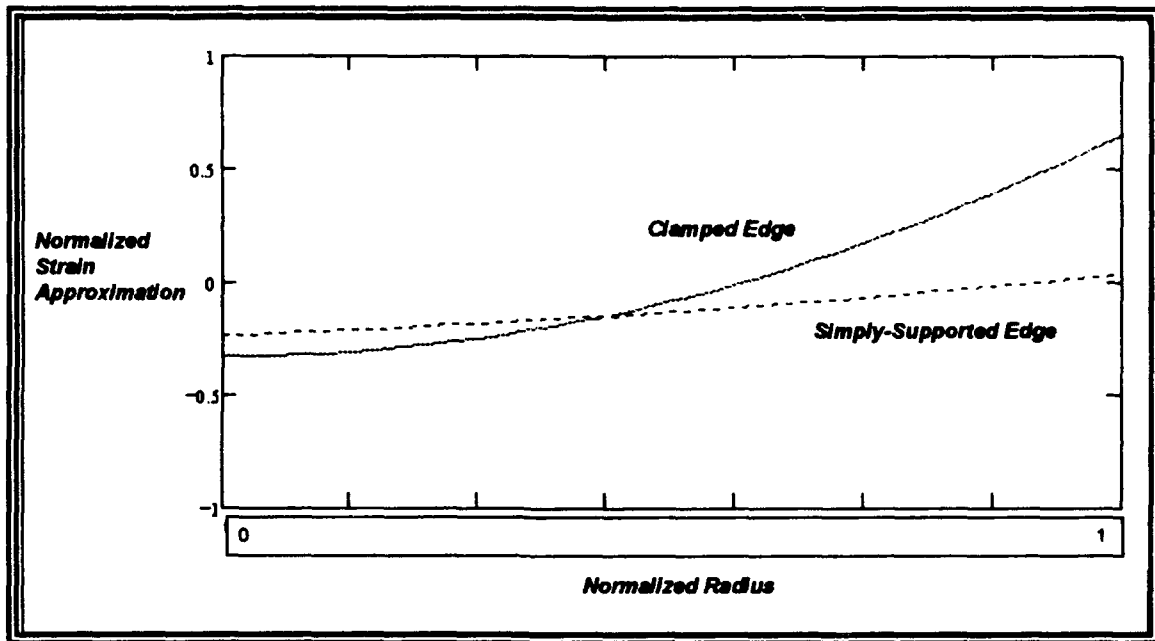strain at the edges increases.

Figure 5 Strain approximation using second derivative of
Curvature.

III. LASER INTERFEROMETRY MEASUREMENTS

This chapter describes the laboratory measurements of the velocity distribution over the transducer's face, radiating in-air, made using a laser doppler vibrometer. These measurements served as the calibration data for the strain gage measurements described in later chapters.

A. THEORY

In-air transducer displacement data was collected in the laboratory using an optical interferometer, the Polytec OFV-350 Laser Doppler Vibrometer. Scattering and attenuation of laser light in water, and the reflection at the water-air boundaries, make the vibrometers use for underwater measurements very difficult, thus the optical method was not used for in-water measurements.

Using a laser beam as the optical source, it is possible to measure displacement magnitudes as small as a wavelength of light, less than one nanometer, which is more than adequate for the intended measurements of transducer displacement.

The technique of interferometry will not be discussed here in detail. The reader is encouraged to consult O'Shea, Callen and Rhodes [Ref. 4] and the Polytec Operators Manual [Ref. 5] for a more detailed description of laser interferometry. In brief, the intensity amplitude of the superposition of two laser beams is measured, one of which

14

has been reflected off the moving object whose velocity is to be measured. Constructive and destructive interference of the added beams causes oscillations in the intensity. A photodetector, housed in an optical sensor head, responds to the intensity of the combined beams. A built-in frequency counter measures the rate of intensity oscillations, which is converted to velocity amplitude. The Polytec OFV-350 makes added use of the doppler shift of the reflected light frequency to determine the direction of motion.

The sensor head provides an output voltage that is proportional to the normal velocity of the object under test. One volt is equivalent to 25 millimeters per second. From the equations of simple harmonic motion, velocity thus calculated can be easily converted by computer to displacement if required.

$$Displacement = A\sin\omega t \qquad (3.1)$$

$$Velocity = A\,\omega\cos\omega t \qquad (3.2)$$

The maximum displacement of the motion, A, at the given frequency is thus

$$A = Velocity\,/\,\omega \qquad (3.3)$$

B. PROCEDURES

The displacement distribution over each projecting face of two flexural disk transducers was measured using the setup depicted in Fig. 6. The individual transducer's faces will be referred to as 44A, 44B, 42A and 42B.

15

Each transducer was attached to a mount, enabling accurate normal velocity measurements to be made. Small cut out dots of adhesive-backed reflective tape were attached to the face of each transducer at one-half centimeter intervals. These dots identify the measurement positions as well as provide strong backscattering of the laser beam. Fig. 7 illustrates the arrangement of transducer mount and reflective dots.

The HP4194 was used to drive the transducer with a sinusoidal signal, sweeping frequencies near the resonant peak of interest (approximately 4100 Hz in air). The (50 ohm) signal output of the HP4194 was fed through a power amplifier with a very low output impedance to maintain a constant voltage drive as the frequency was swept through the transducer's resonance frequency. The output voltage of the amplifier was monitored by a voltmeter, ensuring that a constant voltage was maintained throughout all phases of the experiment. A drive voltage of 2.8V rms proved to be the maximum usable value without the velocimeter output overloading the HP4194. This voltage was sufficient to collect accurate data. An oscilloscope was used to monitor the inputs to the HP4194.

The signal from the vibrometer was input to the test channel of the HP4194, and the transducer drive signal input to the reference channel. A computer program, presented in
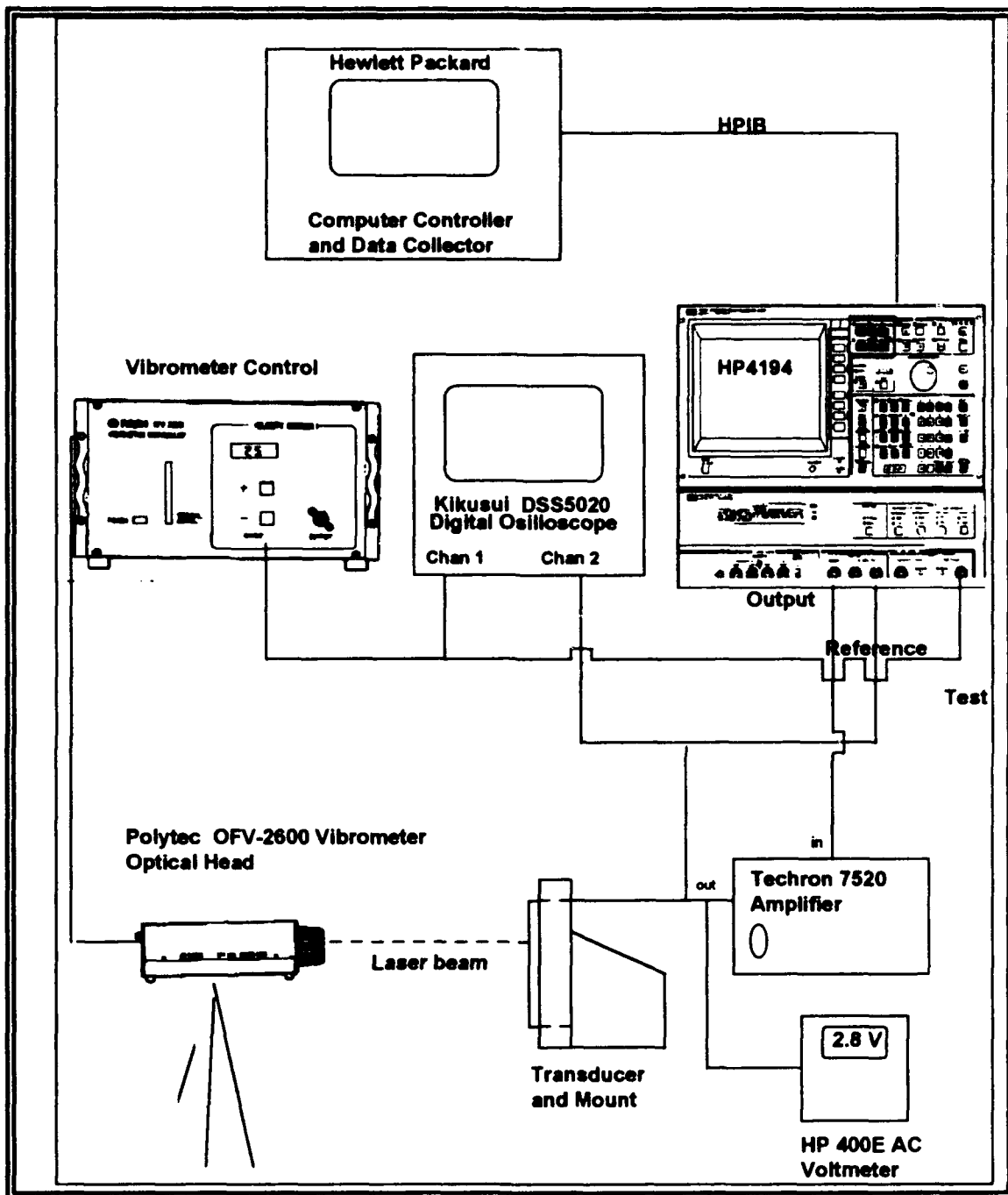
Figure 6 Displacement Measurement Setup.

17
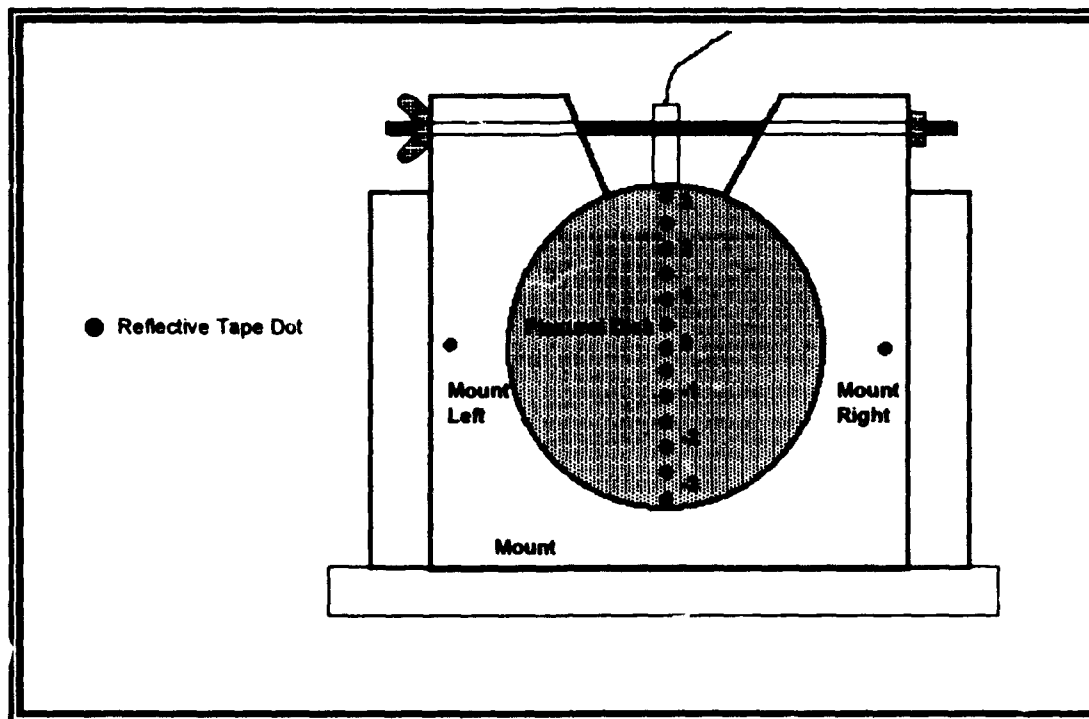
Figure 7 Arrangement of transducer mounting and reflective dots.

Appendix A, was developed and used to control the HP4194, commanding it to drive the transducer through a specified range of frequencies. Use of the computer control simplified the data collection and was a great time saver. The program sets the HP4194 to the Gain/Phase mode and records the voltage gain (test/reference) in dB and the phase shift in degrees.

Data sets were recorded at 401 frequencies, from three to five kHz, at five Hz intervals, for each reflective dot location on the transducer face. Each measured value was computed from the integration of the signal for either 5 or

100 milliseconds, depending on the signal-to-noise ratio. Sixty-four such measurements were automatically made at each frequency and averaged by the HP4194. The data were then stored on a floppy disk for permanent record and for transfer to a personal computer for conversion to displacement and for further analysis (the analysis and processing of all data in this thesis was performed using Mathcad [Ref. 6], a graphical programming language.) This procedure was repeated for each of the 15 measurement points on each face of each transducer.

It was expected that the motion of the outer edges of the transducer, or of the transducer mount, would be zero. However this was not the case. Measurements showed a clear resonant peak, indicating the presence of unwanted movement of the mount, not just electronic noise. Vibration of the mount caused by vibration of the transducer, though very small, was non negligible and had to be subtracted from the transducer face velocity measurements.

To determine the mount vibrations, velocimeter measurements were made of the mount while the transducer was operating. These were then subtracted from the velocity data collected from the transducer face by first converting the magnitude and phase of the measured transducer and mount velocity data to complex form and then subtracting the average of the mount velocity measurements taken on either side of the transducer from the transducer velocity measurement taken at each reflective dot. The resulting

19

data were converted to peak voltage values from rms dB
values and then converted to velocity. These calculations
were performed by the computer program listed in Appendix B.

Fig. 8 illustrates the magnitude and phase of the mount
vibration for transducer 44A. The magnitude of the mount
vibration displacement (3 x 10^-8 meters) was two orders of
magnitude less than that of the displacement at the center
of the disk (3 x 10^-6 meters). However as the displacement
was calculated to 4 decimal places, the vibration movement
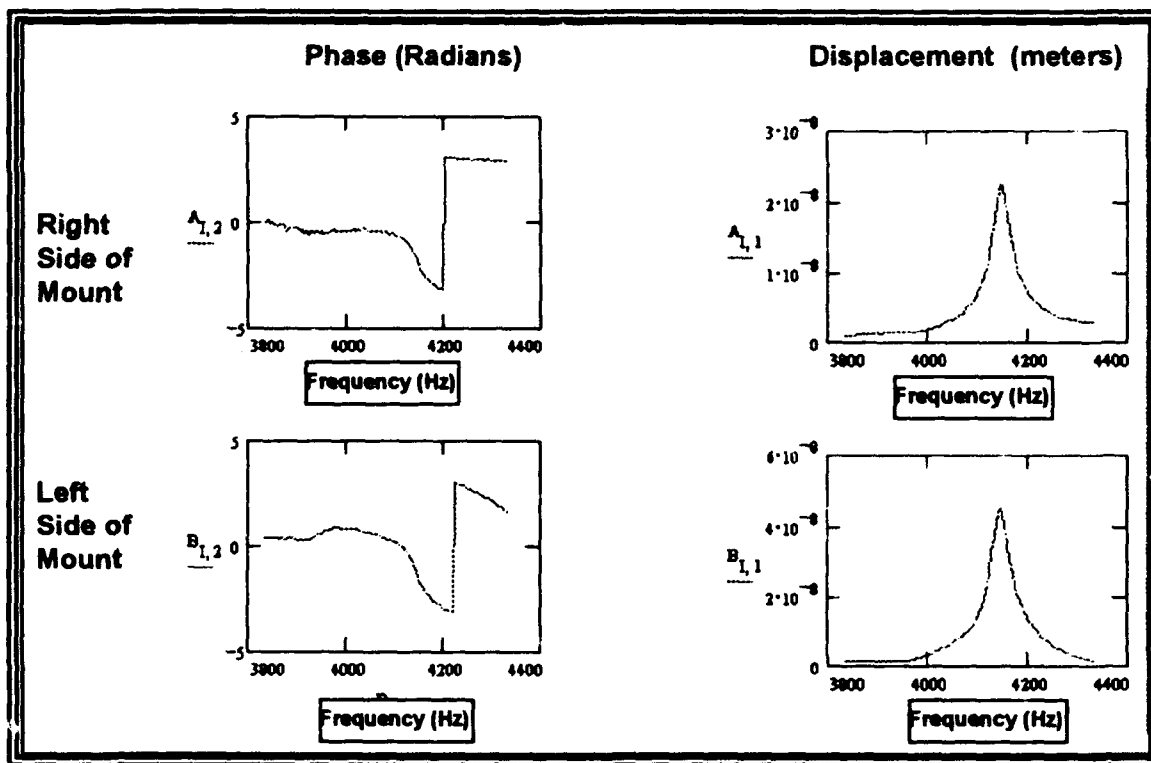was not negligible.

Figure 8 Mount vibration.

Fig. 9 shows the processed results of the displacement measurements for disk 44A, measured at the center reflective dot. The procedure described above was repeated for each reflective dot on each transducer face. The resulting displacement data for each face were then compiled into a single matrix of the form shown in Fig. 10.

Due to the limitations imposed by Mathcad on the matrix size and the lack of measurable vibration at frequencies far from resonance, only data for frequencies within 250 Hz of resonance were considered important and were processed.

C. RESULTS

The following results are for flexural disk 44A. The complete set of results for all the transducers can be found in the appendices. Surface plots of displacement amplitude versus frequency and measurement position proved informative to visually validate the mass of data collected. Fig. 11 show the surface plot formed from the matrix described by Fig. 10, for face 44A. The displacement, as expected, is continuous along both frequency and position axes, showing maximum deflection at the resonance frequency and at the center of the transducer.

A plot of the displacement phase (relative to the drive voltage) versus frequency and position for face 44A is shown in Fig. 12. Phase changes were observed to occur only with
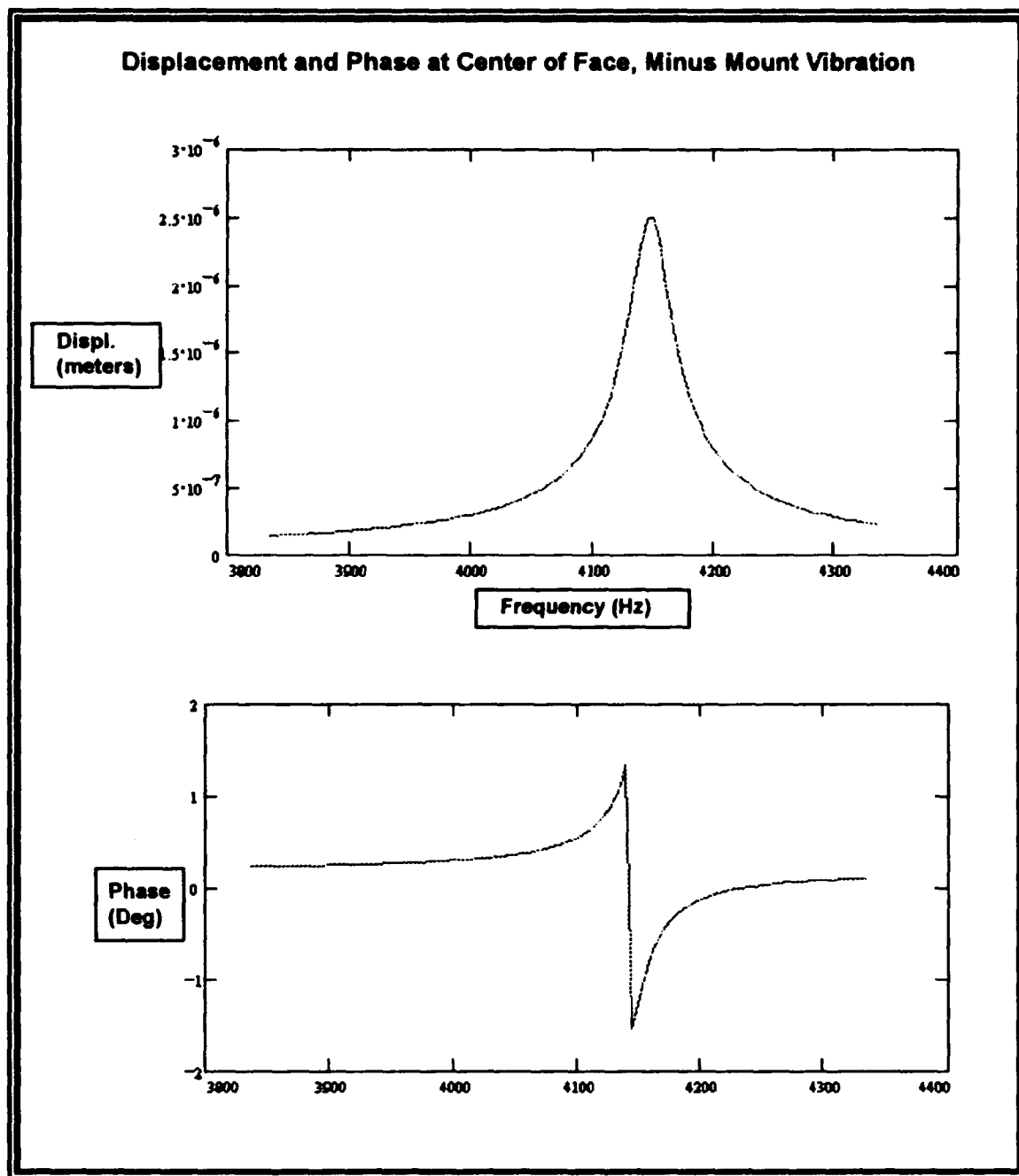
Figure 9 Displacement and phase at center of face, minus mount vibration.

Frequency	Position on Face of Transducer														
	-3.5	-3.0	-2.5	-2.0	-1.5	-1.0	-0.5	0	0.5	1.0	1.5	2.0	2.5	3.0	3.5
3000	—	—	—	—	—	—	—	—	—	—	—	—	—	—	—
3005	—	—	—	—	—	—	—	—	—	—	—	—	—	—	—
3010	—	—	—	—	—	—	—	—	—	—	—	—	—	—	—
—					Displacement and Phase Data										
4990	—	—	—	—	—	—	—	—	—	—	—	—	—	—	—
4995	—	—	—	—	—	—	—	—	—	—	—	—	—	—	—
5000	—	—	—	—	—	—	—	—	—	—	—	—	—	—	—

Figure 10 Form of resultant data matrix.

changes in frequency, not with position along the face of
the disk. This plot visually confirms that the harmonic
motion over the flexural disk face is in phase, as it should
be. The single discontinuity in phase in Fig. 12 is an
artifact of the ambiguity of the actual phase modulo 2π.

D. POLYNOMIAL APPROXIMATION OF DISPLACEMENT

If the deflection of the disks can be represented by a
fourth order polynomial of the form derived in Chapter II.
The displacement should normalize to the same deflection
curve, regardless of displacement's maximum value. To test
this hypothesis, the displacement data versus position
at each frequency was normalized to the maximum value at that
frequency and plotted on the same graph. Fig. 13 shows the
same surface plot as in Fig. 11, but with all data across
the transducer face normalized to the maximum value (for that
frequency) which is located at the center of the disk. Fig.
14 shows the same normalized surface plot looking on end at
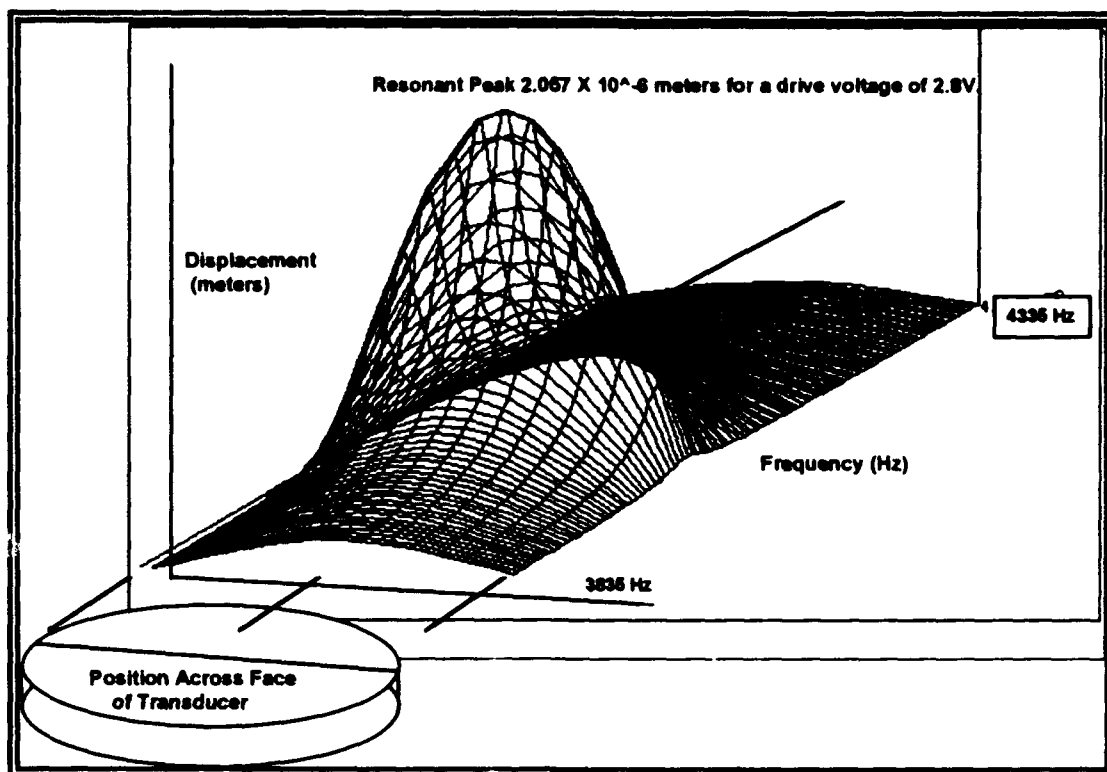the over 1500 data points. This plot makes it clear

Figure 11 Plot of displacement amplitude for face 44A.
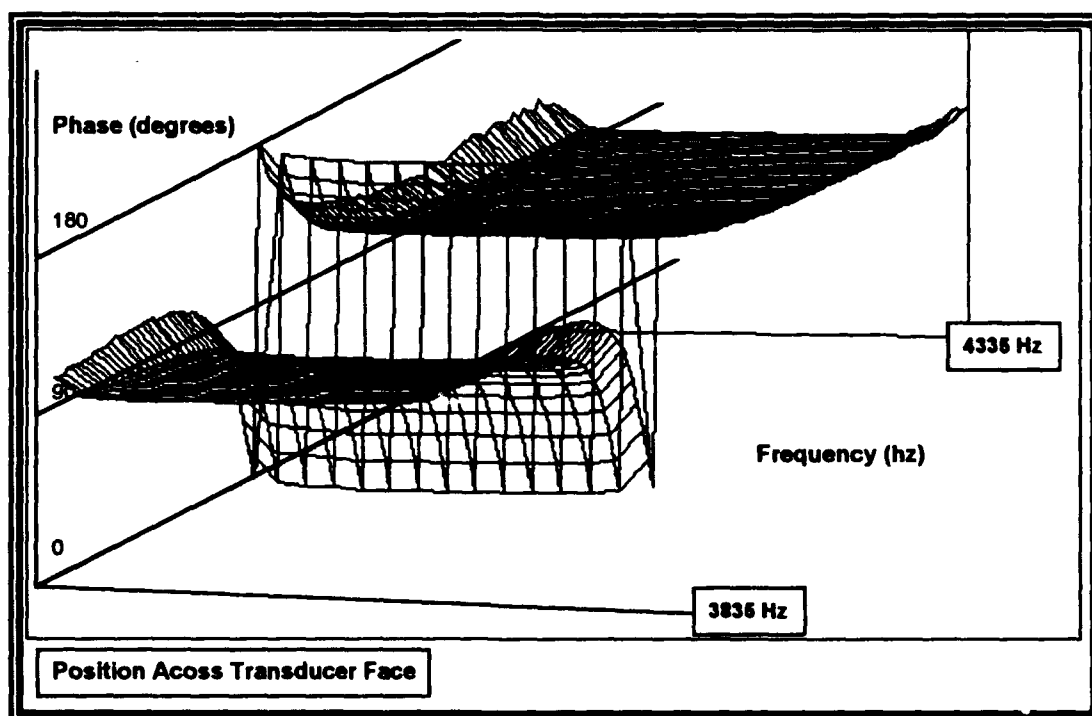

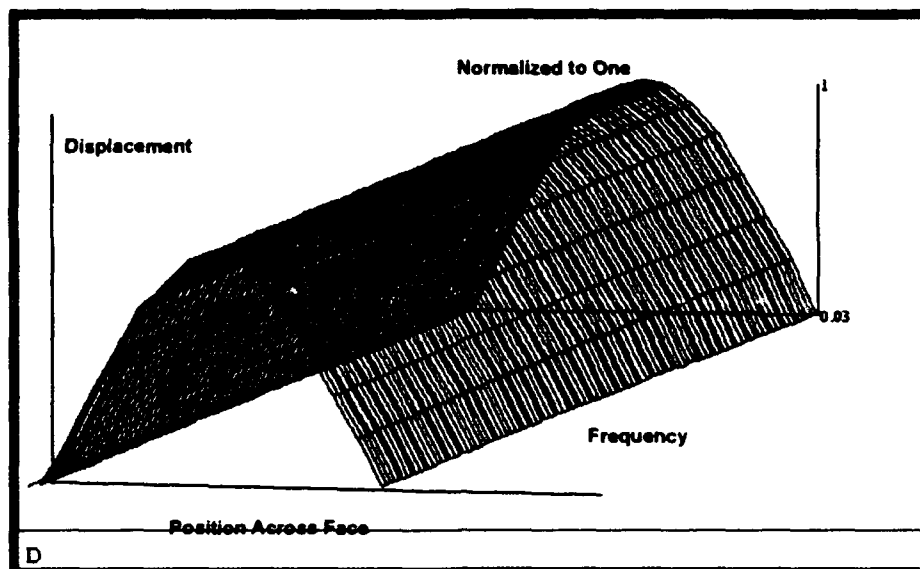**Figure 12** Plot of displacement phase for face 44A.

Figure 13 Normalized displacement.

that the normalized displacement distribution is independent
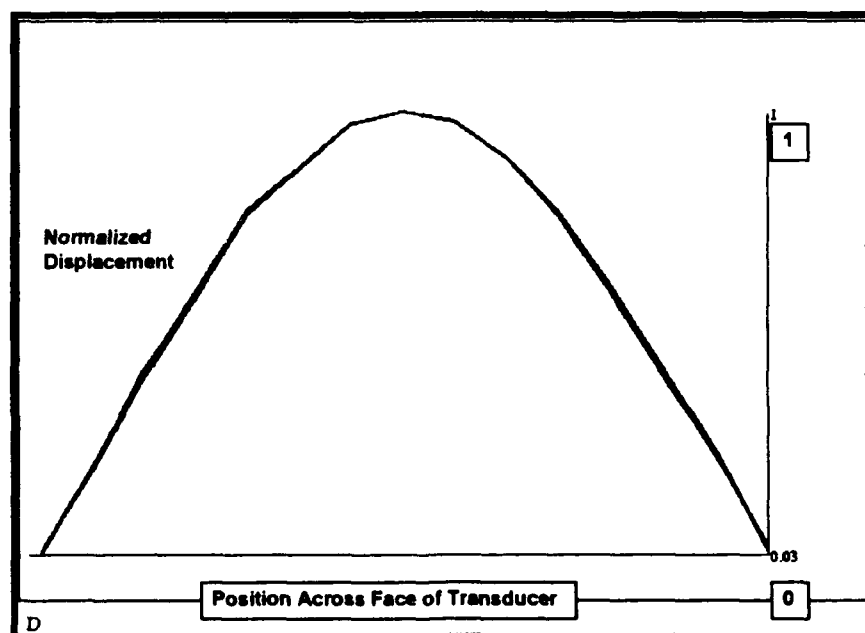of frequency or of the maximum displacement magnitude, at
least in air.

Figure 14 Normalized displacement end view.

Therefore, given the displacement at any point on the transducer face, at any frequency, we can calculate the displacement over the entire face of the transducer.

According to the theory derived in Chapter II, the deflection equation of a flexural disk can be approximated by a fourth order polynomial of the form

$$D(r) = a_0 + a_2 \frac{r^2}{A^2} + a_3 \frac{r^3}{A^3} + a_4 \frac{r^4}{A^4} \qquad (3.4)$$

By using a curve fit program, a fourth order polynomial equation was calculated that best fit the averaged normalized displacement data shown in Fig. 13. The program was allowed to calculate the best fit, not constrained to hold a_1 to zero, to test if the data conforms to the theory. For flexural disk 44A, the best fit equation is as follows (both a_1 and a_3 term were negligable and have been dropped):

$$D(r) = 0.9997 - 1.313 \frac{r^2}{A^2} + 0.3096 \frac{r^4}{A^4} \qquad (3.5)$$

It was found, as expected, that a fourth order polynomial was sufficient to give a very accurate approximation of the measured displacement distribution. Increasing the order of the polynomial equation failed to produce any significant improvement in the fit of the measured displacement curve. The polynomial coefficients are of the magnitude and sign

expected, (see Table 1 and associated text) and the a_1 and the a_3 terms are negligible.

Fig. 15 plots the deflection curves for the theoretical clamped edge, the theoretical simply-supported edge, the actual values for the raw data, and the curve fit. It is clear that the motion of the face conforms very closely to that expected for a simply-supported disk. The coefficient values are very close to the expected values for this case (refer to Table 1). Table 2 presents the polynomial coefficients for each of the disk faces tested.
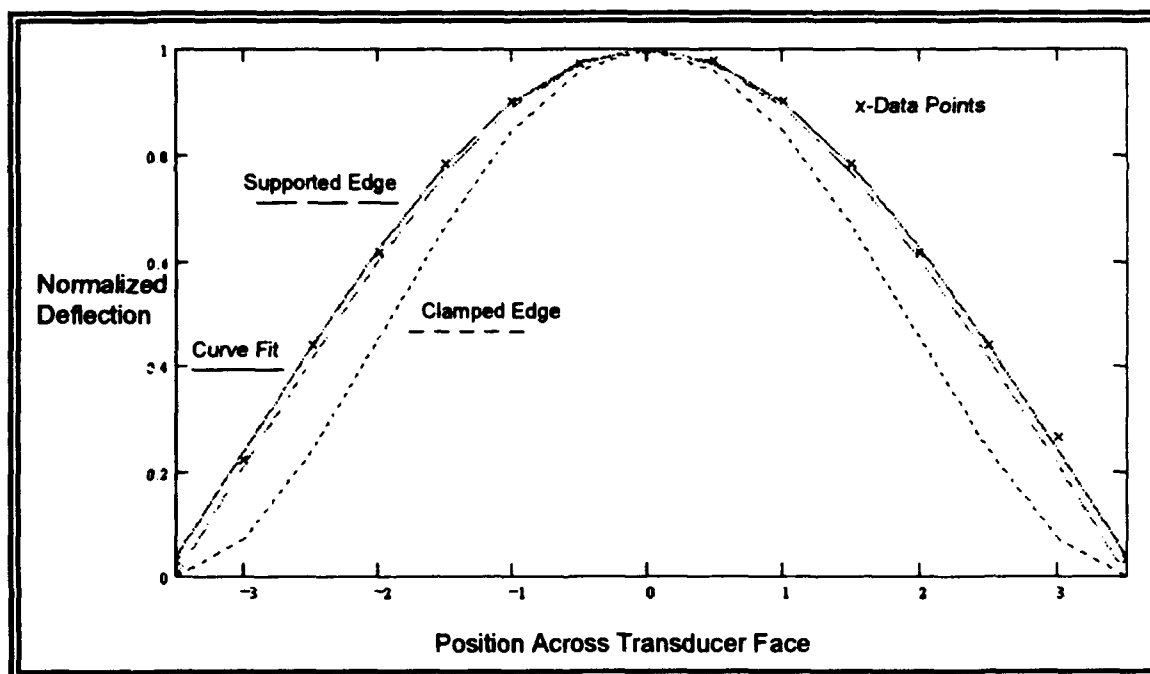
Figure 15 Normalized curves of theoretical, actual, and curve fit displacement.

To calculate the displacement amplitude as a function of r, one must multiply the normalized displacement by the maximum measured displacement.

TABLE 2 COEFFICIENTS FOR TRANSDUCER NORMALIZED DISPLACEMENT CURVES.

	Coefficients			
	a_0	a_2	a_3	a_4
44A	0.9997	-1.313	0.004657	0.3096
44B	0.9898	-1.349	-0.0333	0.3636
42A	1.0006	-1.316	0.00166	0.3077
42B	1.1015	-1.421	0.0163	0.4105

IV. STRAIN MEASUREMENTS

This chapter describes experiments in which the surface strain of the transducer's radiating face was measured using bonded resistance strain gages, and how the strain data were converted can be converted into surface normal displacement.

A. INTRODUCTION

Strain gages are used to measure the surface deformation of an object under stress. A bonded resistance strain gage, such as those used in this experiment, utilizes the change in resistance with length of a serpentine resistor bonded to a plastic film, which is itself bonded to the object under test, to sense the strain in the surface beneath it. A calibration constant for each gage, called the gage factor, relates the strain to the gage resistance.

$$G = \frac{\Delta R / R_0}{\epsilon}$$
(4.1)

where

G = gage factor
ΔR = resistance change in the gage in ohms
R_0 = original or unstrained resistance
ϵ = strain of the surface under the gage

By measuring the change in resistance of a strain gage, the deformation of the measured surface can thus be calculated.

B. STRAIN GAGE SELECTION AND INSTALLATION

Selection of a strain gage for the specific application of this research required consideration of numerous factors such as: the small size of the transducer face (8 centimeters in diameter), the dynamic nature of the experiment, and the short duration of the tests to be conducted. References 7 and 8 discuss details for the strain gages selection process.

A fully encapsulated foil strain gage with a polymide backing and a constantan alloy resistance element was chosen. This type of gage is the most widely used for general purpose strain analysis experiments and could be purchased in the required size and sensitivity at a reasonable cost. The specific polymide backing was selected to match the shear modulus of the steel of the transducer face, permitting complete transmission of the strain from the flexural disk face, through the backing, to the sensing grid.

The installation of a strain gage is an extremely exacting procedure that involves careful preparation and execution. All of the necessary installation tools, accessories, and materials were purchased in a single installation kit from the Measurements Group Inc., the supplier of the strain gages. The kit included all surface

preparation solutions, sandpaper, sterile gauze pads, applicators, cements and catalysts, leadwire solder pads and solder, resin solvents, and a complete set of application tools. An instructional video tape also purchased from the same company proved to be essential for learning the proper technique for installing the gages. The video covers the steps involved in surface preparation, gage bonding, leadwire attachment, and application of protective coatings.

A cyanoacrylic adhesive was used to attach the strain gages to the flexural disk faces after the disk outer coatings were cut away and removed.

C. MEASURING STRAIN

Under most circumstances, a Wheatstone Bridge configuration using a constant voltage source would be used to measure the change in gage resistance. In this experiment, a stable constant current source was available, and was used instead. One major advantage of using a constant current source is that only two wires need to be connected to the strain gage, vice the eight that would be needed if using a constant voltage source and Wheatstone Bridge.

Fig. 17 illustrates a constant current circuit for strain measurements. Given a constant current, I, the voltage drop across the source, V, is dependent on the total resistance

$$V = I(R_g + 2R_L) \tag{4.2}$$

where

R_s = The resistance of the strain gage,

R_L = The resistance in the leadwires.

Although the resistance of the wires, R_L, may change with
temperature, these drifts are negligible, as they change
slowly compared with the resistance changes due to the
transducer oscillations (4000 Hz). Thus, temperature
variations were neglected, and the resistance of the lead
wires were assumed constant. The change in gage resistance
is thus:

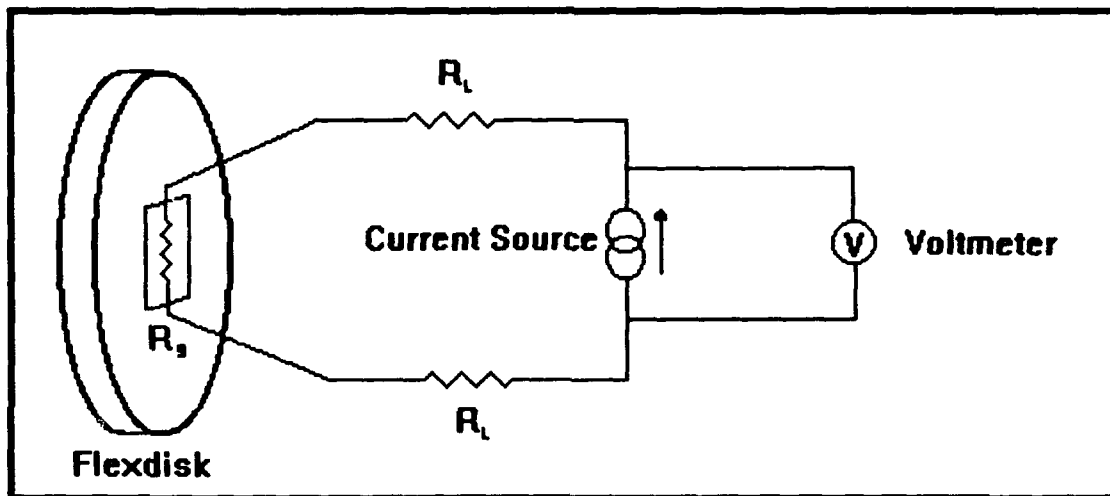$$\Delta V = I\Delta R$$
$$\Delta R = \Delta V / I$$

(4.3, 4.4)

Figure 17 Constant Current Circuit for Flexural Disk Strain
Measurement.

D. EXPERIMENTAL PROCEDURE

Fig. 18 illustrates the setup used to measure the strain at the center of the transducer face. The instrumentation for this portion of the experiment is very similar to that used in the laser measurements except for input to the 4194. A four milliampere constant current source powered by a 24 volt D.C. power supply provided the current to the strain gages. The voltage measured across the current source (sensing strain) was amplified by 1000 using the Ithaco preamplifier and was monitored by the oscilloscope and input to the HP4194. The drive voltage to the transducer was 2.8 volts rms, the same as when the displacement measurements were made. Also the same computer program was used for the strain gage measurements as for the laser vibrometer measurements. A 100 millisecond integration time was used and 16 measurements were averaged at each frequency tested. This arrangement produced clean data sets with very little apparent noise. Tests isolating electronic noise disclosed that, though electronic noise was present, it was not a factor in this experiment.

As with the laser interferometer measurements, the collected data were transferred to the computer via the HPIB interface and stored on a floppy disk for later transferal to a personal computer for analysis and processing. The voltage gain was recorded as a voltage level (dBV) and phase (in degrees).
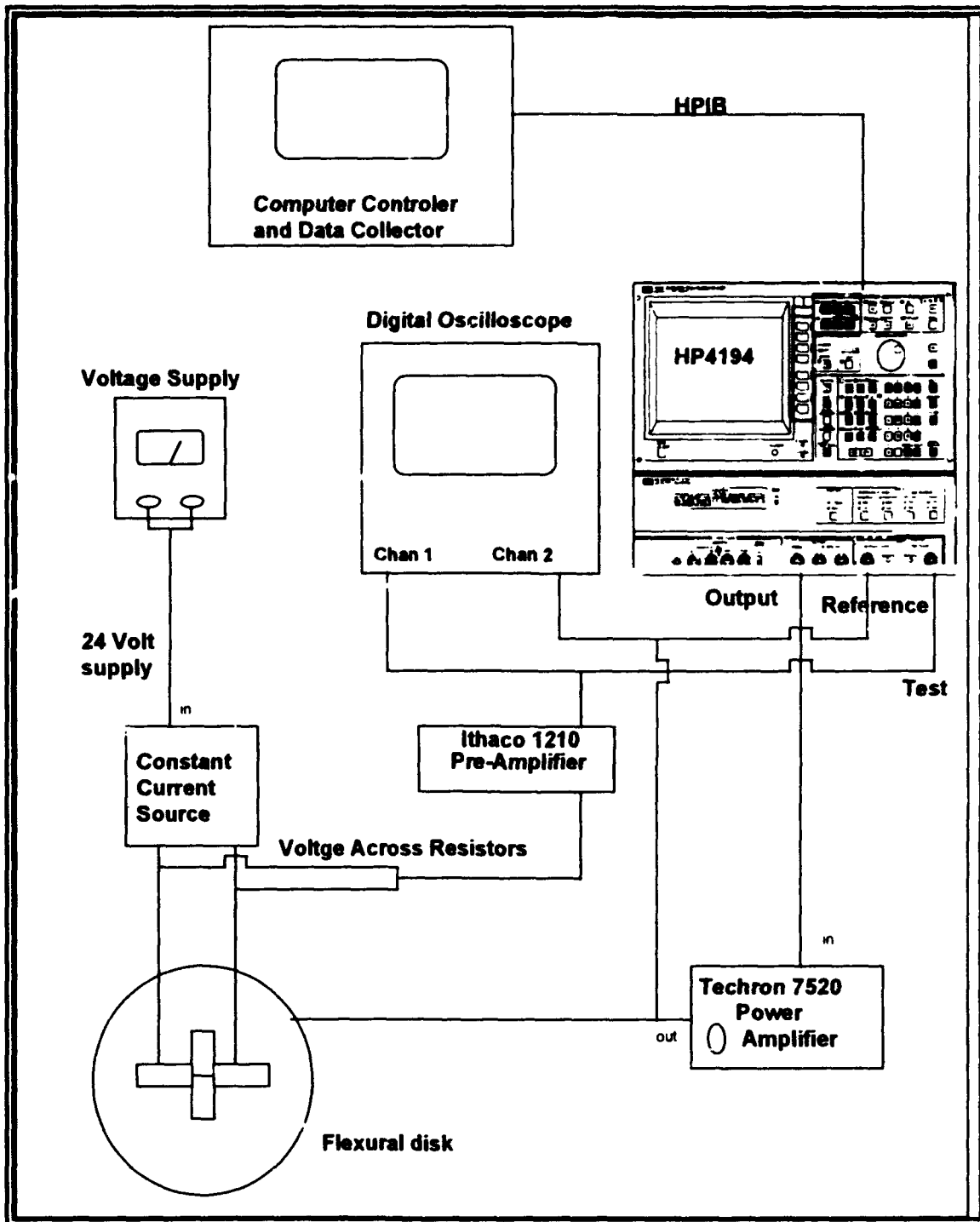
Figure 18 Setup for strain measurements.

E. PRELIMINARY EXPERIMENTS

Three configurations of strain gages were tested to find the optimum placement for maximum voltage output, illustrated in Fig. 19. The first configuration pictured, A, was the one recommended by the manufacturer. It consists of two strain gages oriented to sense the azmuthal strain of the disk surface. The sensitivity of this configuration proved adequate, but not as great as the other two configurations. The following explains why this is so.

Reference 9 discusses stress in a vibrating plate and gives the following relationship between the azmuthal and radial stresses, σ_θ and σ_r,

$$\sigma_\phi = \sigma_r \nu \qquad (4.5)$$

where ν is Poisson's ratio. As Poisson's ratio is less than one-half, generally about 0.3, it is clear that radial stress will be greater than azmuthal stress.
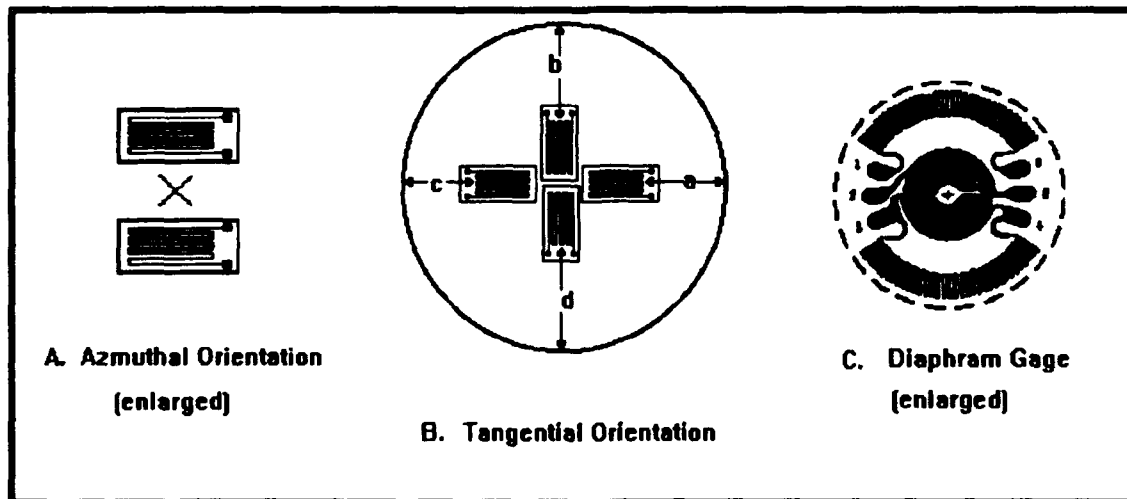

A. Azmuthal Orientation
(enlarged)

B. Tangential Orientation

C. Diaphram Gage
(enlarged)

Figure 19 Strain Gage Attachment Configurations.

For the small strains measured here, stress and strain are proportional. Therefore one can expect that measuring azmuthal strain will be less effective than measuring radial strain. The other two gage placements, B and C, measure radial strain.

Gage C is a diaphragm gage. It was mounted at the center of the disk. Diaphragm gages are normally used to sense the pressure acting on a very small diaphragm. A diaphragm gage consists of four small grids, two in the center, oriented to sense circumferential strain and two outside of these, oriented to sense radial strain. Though normally used with a Wheatstone Bridge, in this test the four 350 ohm grids were connected in series to form one 1400 ohm gage and the gage voltage measured with a constant current applied. These gages proved to be extremely hard to work with. The soldering of the leads required a surgeon's precision due to their small size, and resulted in numerous ruined gages. Since the diaphragm gages are much more expensive then general purpose strain gages and did not provide as large a signal as the second configuration shown, B, they were not used.

Configuration B provided the best signal and was used for subsequent tests. It consists of four identical 350-ohm, parallel-grid strain gages (Micro-Measure, type CEA-06-250UW-350) connected in series to form one 1400-ohm gage. The gages were mounted as close to the center as possible, and oriented radially 90 degrees to one another. Four gages

provided a larger signal than did two gages, as the added
resistance doubled the signal voltage.

The distance from the outside edge of the transducer
face to the outside edge of each gage's sensing grids was
measured and is listed in Table 3. The radius of each disk
is 3.595 cm and the length of each sensing grid is 0.65 cm.

TABLE 3   EDGE TO GAGE DISTANCES

Disk Face	a	b	c	d
42A	2.72 cm	2.46 cm	2.64 cm	2.18
42B	2.72 cm	2.36 cm	2.66 cm	2.12
44A	2.65 cm	2.29 cm	2.73 cm	2.39
44B	2.70 cm	2.28 cm	2.60 cm	2.29

F. RESULTS

Final strain measurements were taken on each transducer
face using gages mounted in configuration B described in the
previous section. The collected data were converted from
voltage level to strain on a personal computer using the
Mathcad program described earlier and listed in the
Appendix. After the rms voltage level was converted to peak
volts, the peak strain at each frequency was calculated
using the gage factor, G,

$$\epsilon = \frac{\Delta R}{R*G} \tag{4.6}$$

where

37

$$\Delta R = \frac{\Delta V}{I} \qquad (4.7)$$

$R = 1400\text{-ohms}$

$G = 2.095$

$I = .004 \text{ A}$

$$\epsilon = \frac{\Delta V}{C} \qquad (4.8)$$

Combining terms

$$\epsilon = \frac{\Delta V}{C} \qquad (4.9)$$

where

$C = \dfrac{I}{R*G}$ and ΔV is the measured output.

Fig. 20 shows the resulting strain versus frequency for each of the transducer faces tested. One can readily see that the strain for face 42B is greater than that of the other faces. Table 4 compares the maximum measured strain to the maximum measured displacement, the ratio being shown in column three. Note that both the observed maximum strain and displacement are the greatest for face 42B. The differences in the observed maximum displacements may be caused by variations in the construction of the laminar disks and/or in the mounting of each disk to its ring. The differences in the displacement-to-strain ratio are probably due to variations in the strain gage mounting conditions.
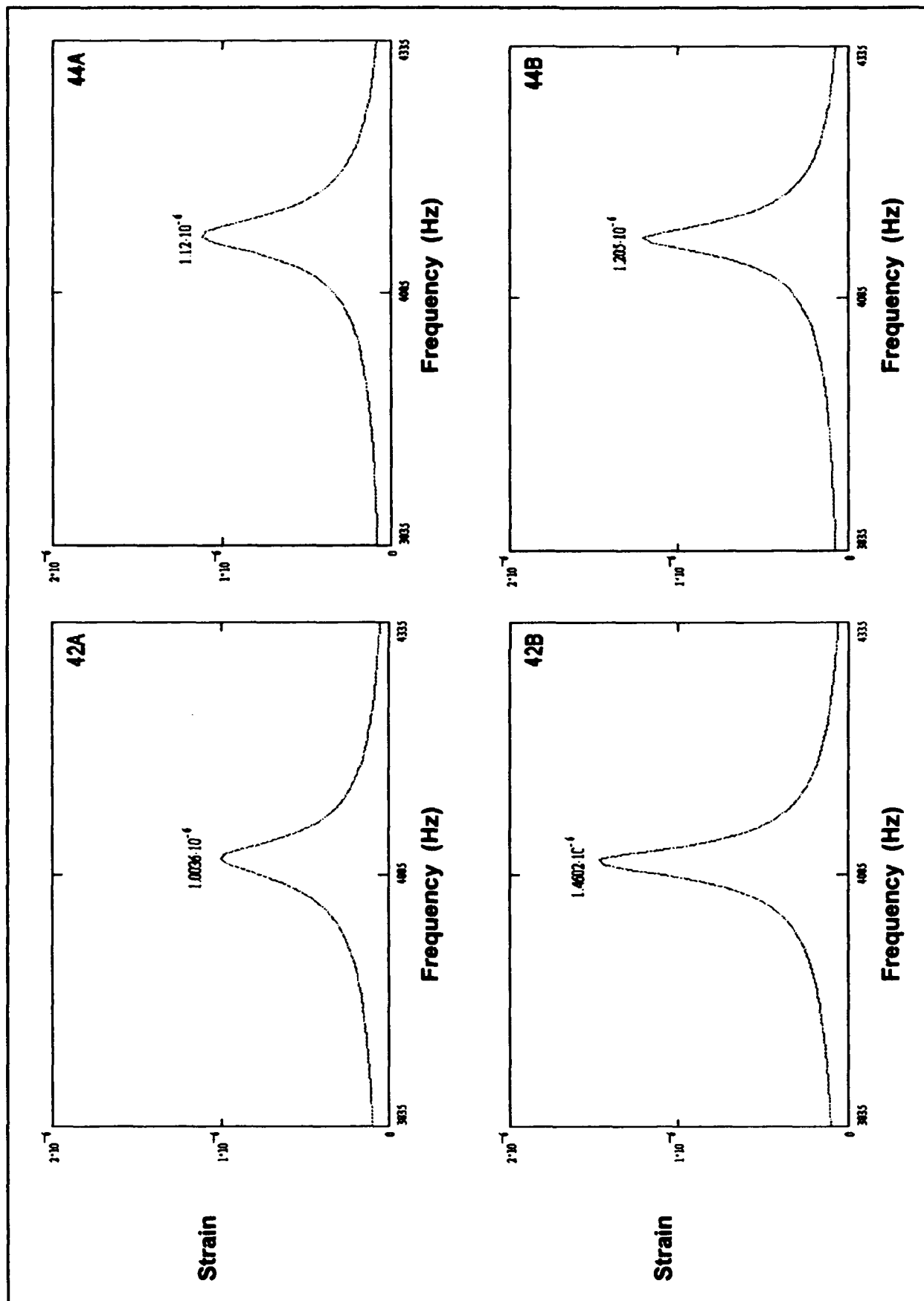
Figure 20 Measured Strain versus Frequency.

TABLE 4 MAXIMUM STRAIN AND DISPLACEMENT

	Max. Strain	Max. Displacement	Displacement/Strain
42A	.001003	2.526 x10^-6	.0026
42B	.001401	2.951 x10^-6	.0021
44A	.001119	2.507 x 10^-6	.0022
44B	.001204	2.715 x 10^-6	.0023

G. VALIDATING PROPORTIONALITY OF STRAIN AND DISPLACEMENT

Since the theory of flexural vibrations is linear, the strain at a point should be proportional to the displacement at that point. A quick and visual method of experimentally confirming this is to compare the normalized strain of the flexural disk obtained from the strain gage measurements, with the normalized displacement obtained from the laser vibrometer measurements taken at the center of the disk over the range of frequencies studied. If the two are proportional, then these curves should be the same. Fig. 21 illustrates the normalized strain and displacement data for flexural disk face 44A. The plots of the other disks can be found in the appendices. The nearly exact match of the two curves confirms that the strain and displacement are proportional to one another and also provides added confidence that both sets of data are accurate. It is now evident that given the measured strain output voltage, V_g,
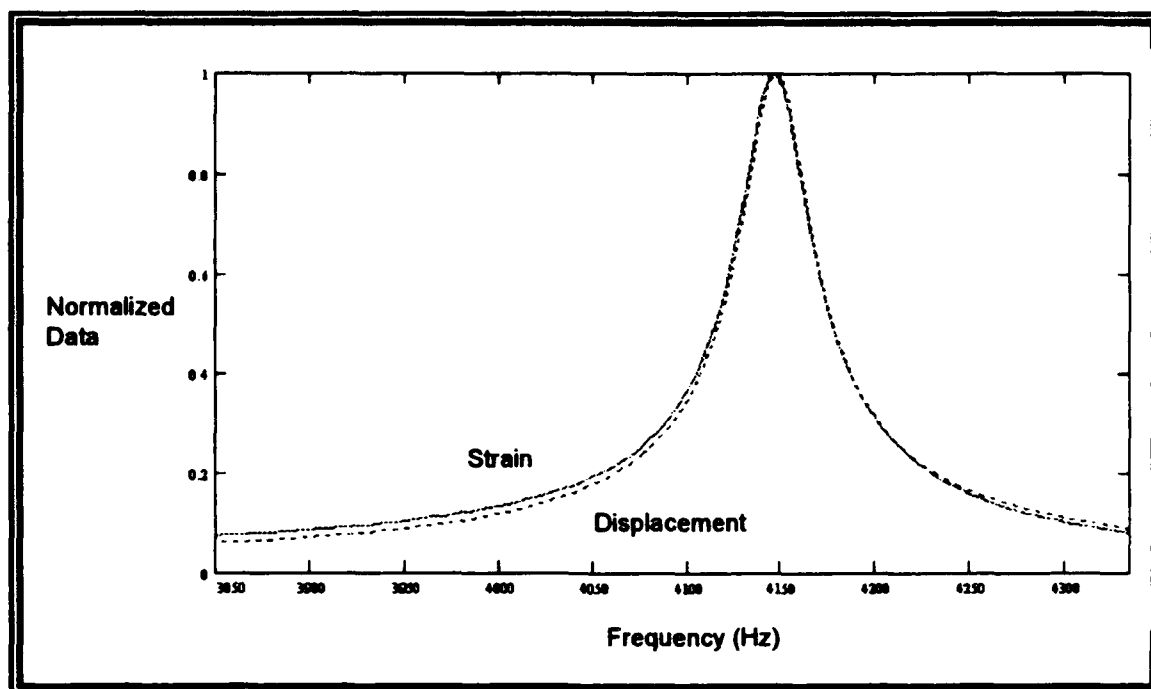
Figure 21 Comparison of Normalized Strain and Displacement.

we can compute the central displacement.

$$D(0) = K * V_g \qquad (4.10)$$

That is, the displacement at $r=0$ is proportional to the strain gage output voltage. At this point the proportionality constant K can be calculated by the equation

$$K = \frac{D(0)}{V_g} \qquad (4.11)$$

using the previously measured maximum displacement, $D(0)$, and the measured strain voltage output V_g. Using this value for the maximum displacement, the deflection curve derived in Chapter Three can be used to describe the displacement over the entire face of the transducer.

41

H. NON-SYMMETRIC FLEXURE

Thus far it has been assumed that the deflection of the disk remains symmetric under all loading conditions. To monitor this, two additional strain gages were mounted at either edge of the flexural disks, as shown in Fig. 22. By measuring the strains at the edges and at the center it is possible to detect non symmetric flexure, if it is large enough. If the deflection is not symmetric, then the deflection curves derived in Chapter III are not valid. No measurable non symmetric vibration was found in any experiments conducted.
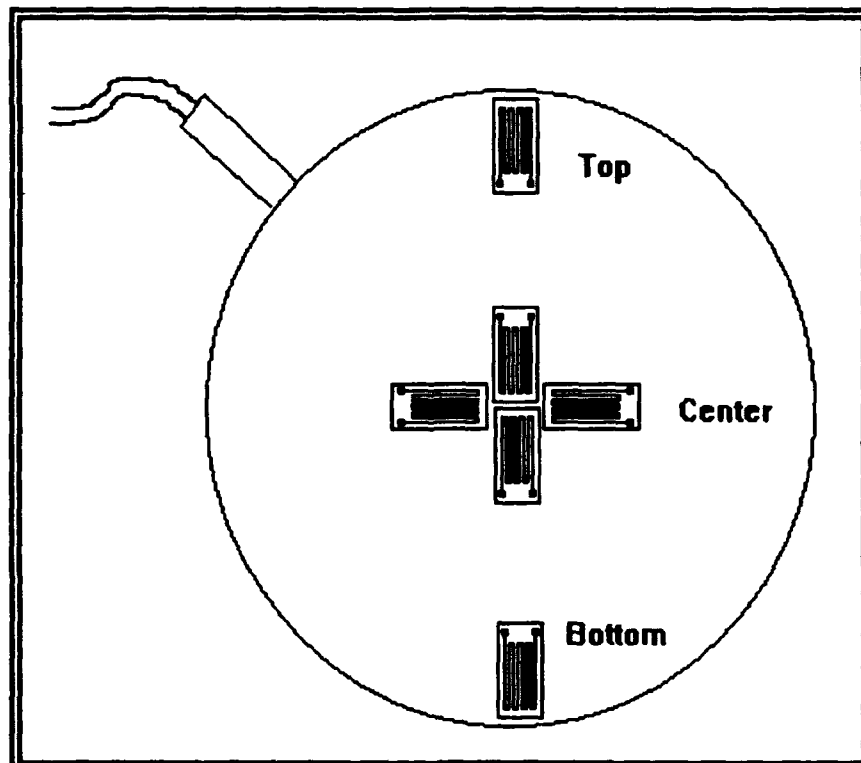

Figure 22 Strain Gage Configuration with Edge Gages.

VI. UNDERWATER MEASUREMENTS

A. INTRODUCTION

The final experiment undertaken in this research
involved the measurement of strain of the flexural disk
surfaces while submerged in the Naval Postgraduate School
acoustic testing water tanks. The goal of this experiment
was to establish the feasibility of investigating the
interaction of closely spaced array elements through surface
strain measurements. A detailed analysis of the interactions
of the two elements will not be attempted here.

The two transducers were tested in the two element array
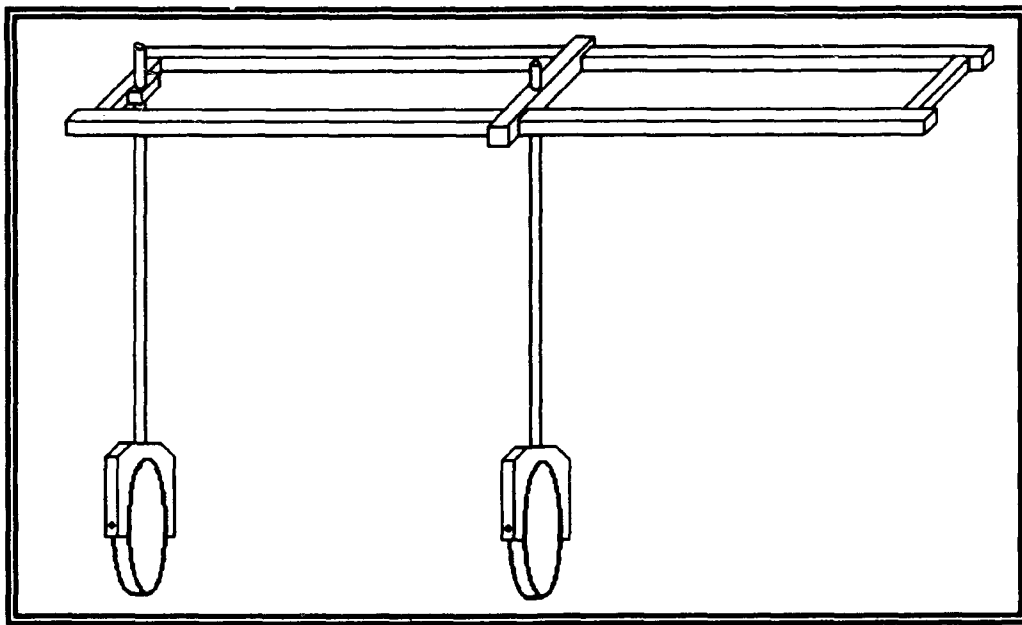configuration depicted in Fig. 23.

Figure 23 Submerged testing apparatus.

The testing apparatus incorporates a graduated track
that allows testing of the two elements at various inter-

element distances. The two elements were mounted using lexan yokes attached to aluminum rods. Lexan, which has a characteristic impedance close to that of water, was used to reduce scattering.

The apparatus allows for the testing of the two disks either face-to-face, as depicted in Fig. 23 or edge-to-edge as in Fig. 24. The first arrangement places the measured
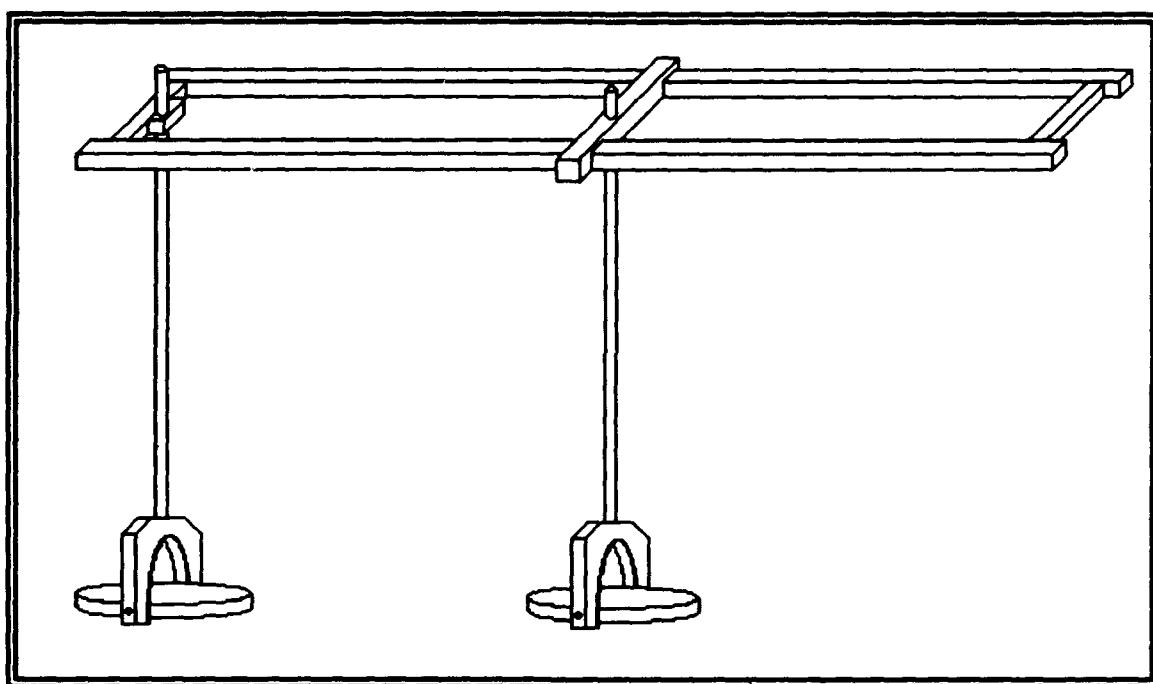
Figure 24 End to end testing arrangement.

disk in a position of symmetrical loading, and the deformation curves derived will be assumed to be valid for this case. The second arrangement places the elements in a position of possible asymmetric loading. Although at the frequencies of operation these elements can be considered to be omni-directional, the two edge monitoring strain gages

44

can be used to indicate any asymmetric flexure of the flexural disk, provided that they are sensitive enough to register the extremely small strains expected in the water. In the event of asymmetric deformation, the deformation curves derived will not apply and can not be used. Due to time constraints, measurements were not made in this configuration; these will be left for the future.

B. PROCEDURES

A simple experiment was performed to establish the feasibility of using surface strain measurements to investigate the effect of one transducer on another. One transducer was driven while the surface strain of a second, undriven transducer was measured. The powered transducer was driven with 28 volts rms (see Fig. 18). The procedure described in Chapter IV was repeated with the exception that the pre-amplifier and the oscilloscope were eliminated. It was discovered these were a source of electronic crosstalk in the measurements. The tests were conducted over a frequency range of 2000 Hertz, from 2500 to 4500 Hertz. The distance between the two transducers was different for each test run. The distances were 3.6, 7.2, 10.8, and 14.4 centimeters, corresponding to 0.5, 1, 1.5, and 2 times the radiating surface radius, receptively. The resulting curves for the measured strain for flexural disk 42A are depicted in Fig. 25.
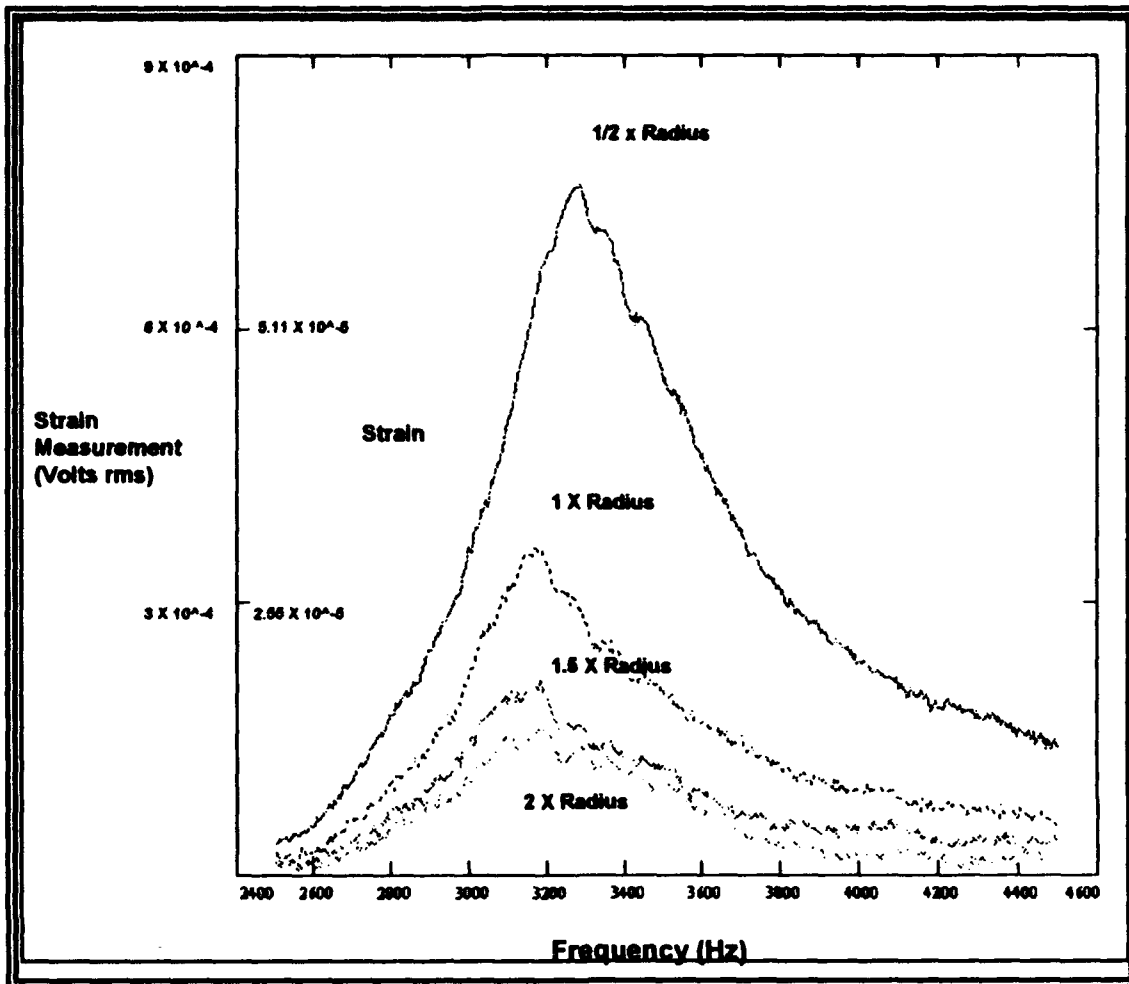
Figure 25 Strain Measurement of Flexural Disk 42A Driven
Externally at Various Distances.

As expected, it is seen that the range between the two
transducers increases, the deflection decreases. This
simple experiment demonstrates the feasibility of the method
of using strain gages to measure displacement of a submerged
transducer.

VI. SUMMARY, CONCLUSIONS, AND RECOMMENDATIONS

A. SUMMARY

1. Measurements were made to map the displacement distribution of the faces of two flexural disk transducers using a laser doppler vibrometer. Deflection curves for each flexural disk face were computed.

2. The same two flexural disks were instrumented with strain gages and measurements of surface strain were made.

3. The proportionality between surface strain and displacement were investigated.

4. Underwater experiments were conducted to demonstrate the feasibility of taking strain measurements submerged that could be used to calculate displacement.

B. CONCLUSIONS

It has been shown that the use of strain gages to measure the displacement of the surface of a transducer is practical. This technique can provide a useful means of determining the deflection of a submerged transducer.

Strain measurements have some inherent difficulties and so great care must be taken to obtain accurate results. The signal sensed is generally extremely small and must be processed and integrated to be of any use. The signal is so small in some situations that noise and electrical crosstalk can become important, so that extreme care must be taken to

eliminate them. Calibration of strain gages using a standard such as a laser interferometer must be performed very carefully. For example, mount vibration needs to be subtracted out.

Despite these limitations strain gages can be very useful where there is a clearly established relationship between the measured strain and the displacement distribution.

C. RECOMMENDATIONS

1. Underwater Work

There remains more work to be done on the calibration of the strain gages and on underwater measurements. More underwater strain gage data needs to be collected. The equipment seemed much more susceptible to grounding problems and electronic noise during the underwater experiments.

2. Rosette Gages

The installation of the strain gages would be much easier and their signal greater if rosette gages, as depicted in Fig. 26, were used instead of the more complex strain gage arrangement used in this experiment. This should provide a similar radial strain measurement capability without the need to apply multiple gages. The rosette could also be wired in series, providing a 1050 ohm gage. With a rosette gage, accurate measurement of the positions of each separate grid is unnecessary.
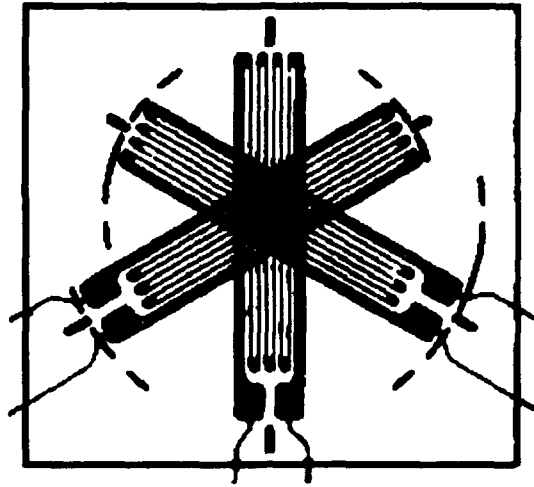
Figure 26 Rosette Strain Gage.

3. Encapsulation

An ideal process for installation of strain gages that would ensure watertight integrity would be to bond the gages to the flexural disk prior to encapsulating in polyurethane. This would greatly simplify the waterproofing of the gages, but would need to be done by the manufacturer. If this is not possible, then the use of a common silicone cement is preferred. The butile rubber used in the present experiments would shrink after application, creating air voids in any cavity, such as the spaces under the wire leads, and pulling on the fragile strain gage leads. A silicone cement does not shrink, has a higher viscosity, allowing it to be worked easier, and adheres to the flexural disk face and wire leads better. Care would need to be taken to prevent the formation of air bubbles during the application of the silicone cement.

APPENDIX A

This appendix contains the computer code for the program "STRMEAS" that was written to control the HP4194 for the experiments in this thesis.

The code is written in HTbasic Version 3.2. The reader with experience in BASIC or PASCAL will find the interpretation straightforward.

```
1        ! PROGRAM STRMEAS
10       !*****************************************************************
40       !*              MEASURING GAIN PHASE WITH THE                  *
50       !*                      HP4194                                 *
60       !*         Douglas L. Cuthbert   - January 1993                *
70       !*           NAVAL POSTGRADUATE SCHOOL                         *
80       !*           MONTEREY, CA 93943   USA                          *
90       !*                                                             *
100      !*****************************************************************
110      !
120      !
140      !*************************
150      !*   INITIAL CONDITIONS   *
160      !*************************
170      OPTION BASE 1
180      ASSIGN @Analyzer TO 717
190      MASS STORAGE IS ":,700,0,6"
200      Clear$=CHR$(255)&CHR$(75)
210      Home$=CHR$(255)&CHR$(84)
220      !
460      !****************************************
470      !*   VARIABLE INITIALIZATION   *
480      !****************************************
530      !
540      DIM A_data(401),B_data(401),Freq(401)
600      INTEGER I,Nop,Number
630      !
640      !*****************************************************************
650      !************** MAIN PROGRAM  ****************
660      !*****************************************************************
670 Start:       !
680     GOSUB Pgm_init                          ! Program initialization
690        !
770        !** performing the measure **
790        GOSUB Measure
800        !
810        !** reading datas from the ANALYZER to the system **
820        !
860           OUTPUT @Analyzer;"NOP?"           ! Query 4194 for # of data points
870           ENTER @Analyzer;Nop               ! Reading number of points
890           !
900           REDIM A_data(Nop),B_data(Nop)     !,C_data(Nop),D_data(Nop)
910           REDIM Freq(Nop)
920           OUTPUT @Analyzer;"X?"             ! Query 4194 for frequency
930           ENTER @Analyzer;Freq(*)           ! Reading frequency
970           OUTPUT @Analyzer;"A?"             ! Query for gain, than a
980           ENTER @Analyzer;A_data(*)
990           OUTPUT @Analyzer;"B?"             ! Query for Phase, than b
1000          ENTER @Analyzer;B_data(*)
```

```
1100  !
1110  !
1120  !**********************************************************************
1130  !***************      DATA STORAGE      ***************
1140  !**********************************************************************
1150  !INPUT "Store data to a floppy disl and hard drive?  Y/N  ?",Answer$
1160  !IF Answer$="Y" OR Answer$="y" THEN
1161    MASS STORAGE IS ":,700,1"
1170     PRINT
1190     PRINT
1203     CREATE BDAT Filename$,Nop
1212     ASSIGN @Path TO Filename$;FORMAT ON
1240     FOR I=1 TO Nop
1270     OUTPUT @Path;Freq(I),A_data(I),B_data(I)
1350     NEXT I
1360     MASS STORAGE IS ":,700,0,6"
1370  !END IF
1380   GOTO The_end
1390  !
1400  !**********************************************************************
1410  !*********SUBROUTINES ***************
1420  !**********************************************************************
1430  !
1440 Pgm_init:                         ! PROGAM INITIALIZATION
1450   OUTPUT KBD;Clear$
1460   OUTPUT KBD;Home$
1470   PRINT "BEGINNING ..."
1480 RETURN
1490  !
1500  !.................................................
1510  !
1520 Measure:                          ! PERFORM A MEASUREMENT
1530   PRINT
1550   DISP "ENSURE  SETUP IS COMPLETE, Press CONTINUE when ready."
1560   PAUSE
1562   CAT ":,700,1"
1565     INPUT "ENTER FILENAME, Type-#-Voltage-Position, ",Filename$    ! Read fil
1566     PRINT Filename$
1570   DISP ""
1580   GOSUB Anl_init
1590   GOSUB Sweep
1650 RETURN
1671  !.................................................
1672  !This is the section to change if you require different settings
1673  !                  on the HP4194
1674  !.................................................
1680  !
1690 Anl_init:                         !ANALYZER INITIALIZATION
1700   PRINT "++initializing HP4194++"
1710   CLEAR @Analyzer                  !initialize the HP 4194A
1720   WAIT 2.0
1760   OUTPUT @Analyzer;"SWM2"          !Single sweep mode
1790   OUTPUT @Analyzer;"PWS2"          !power splitter to single mode
1800   OUTPUT @Analyzer;"ZIR1;ZIT1"     !channels input impedance to 1MOHM
1801   OUTPUT @Analyzer;"ATT2;ATR2"     !attenuation to 20 dB
1830   OUTPUT @Analyzer;"FNC2"          !GAIN-PHASE measurements
1840   OUTPUT @Analyzer;"GPP1"          !TCH/RCH
1850   OUTPUT @Analyzer;"ITM2"          !medium integration time
```

52

```
1890   OUTPUT @Analyzer;"OSC=1V"              !osc level   1 "
1900   OUTPUT @Analyzer;"START=3000HZ"        !Frequency start = 3000H-
1910   OUTPUT @Analyzer;"STOP=5000HZ"         !Frequency stop = 5KHz
1920   OUTPUT @Analyzer;"NOA=16"              !Averaging number = 16
1960 RETURN
1980   !....................................................................
1990   !
2000 Sweep:                                  ! ENABLE MEASUREMENTS
2010   PRINT "!! start sweep !!"
2020   OUTPUT @Analyzer;"SWTRG"               !Sweep start trigger
2030   BEEP 900,.1
2040   LOOP
2050     EXIT IF PINAND(SPOLL(@Analyzer),2) !waitting for the end of measurements
2060   END LOOP
2070   BEEP 900,.1
2090 RETURN
2110   !....................................................................
2120   !
2310   !
2320 The_end: !
2330   !
2340   LOCAL @Analyzer                        !Return control to the front panel
2350   !
2370   BEEP 2000,.3
2380   BEEP 800,.2
2390   PRINT
2450   PRINT "********************************************************************"
2451   PRINT "              END OF MEASUREMENT"
2460   PRINT "********************************************************************"
2470   BEEP 2000,.15
2480   END
```

APPENDIX B

This appendix contains results of the experiments on flexural disk 42A. All of the calculations are performed using Mathcad and are discussed in the text.

Surface plots of displacement and phase   FD42A
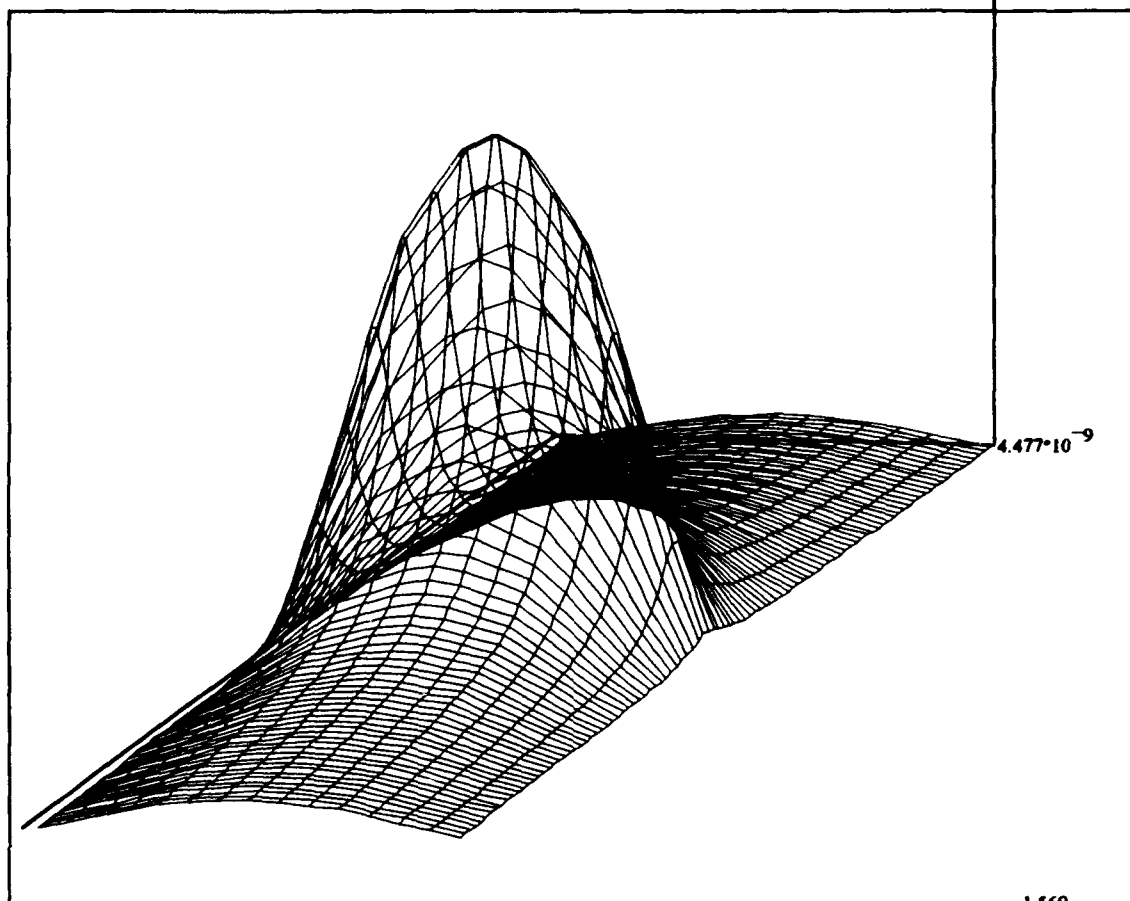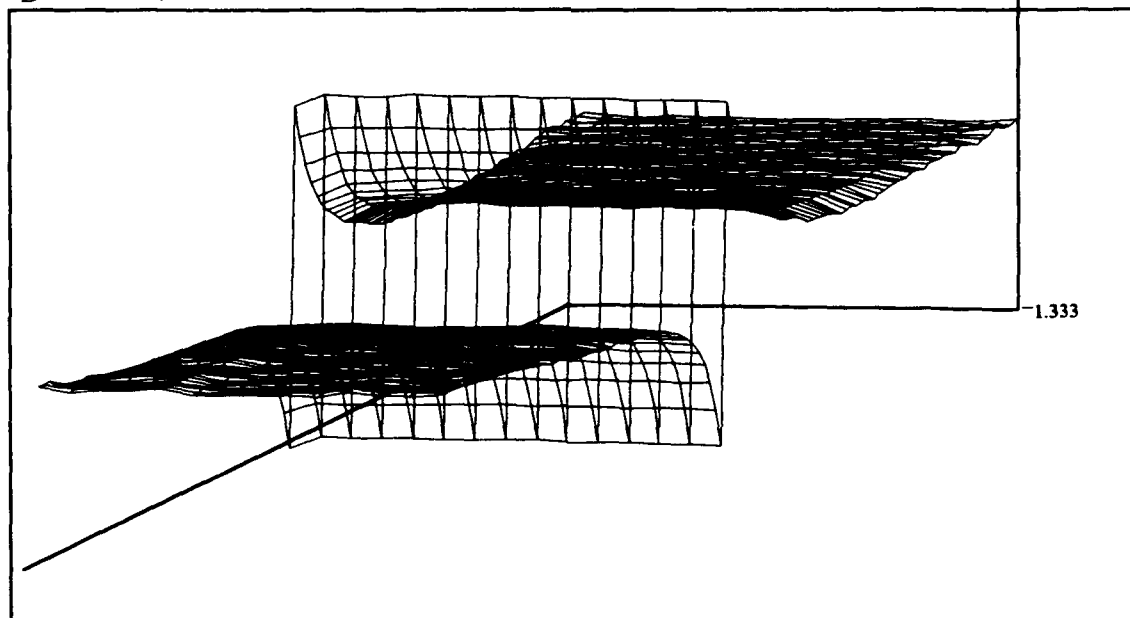
Normalization of Displacement Data

FD42A, 2.8 Volts

$D := READPRN(D)$

Normalize all data for each frequency to the max value

$rows(D) = 101$ $\qquad cols(D) = 15$ $\qquad max(D) = 2.526 \cdot 10^{-6}$

$J := 0 .. 100$ $\qquad I := 0 .. 14$ $\qquad M := max(D)$ $\qquad M = 2.526 \cdot 10^{-6}$

$D := D^{T}$

$M_J := max\left(D^{<J>}\right)$ $\qquad D_{I,J} := \dfrac{D_{I,J}}{M_J}$
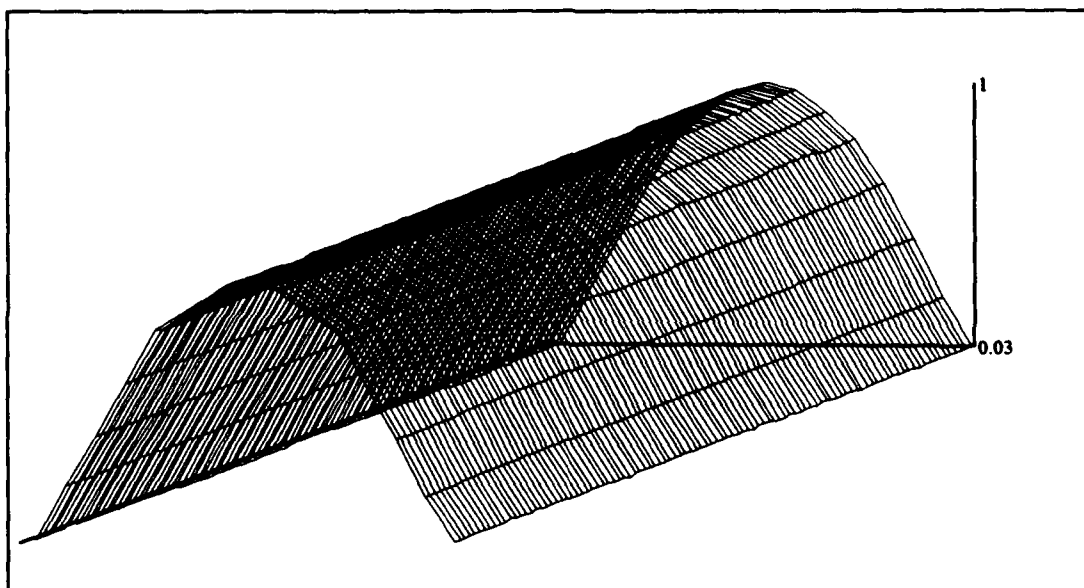
$\qquad\qquad Ndispl_{I,0} := \dfrac{I}{2} - 3.5$ $\qquad Ndispl_{I,1} := D_{I,7}$ $\qquad WRITEPRN(NDispl) := Ndispl$

$D := D^{T}$

D

Viewing the same plot on end

D

56
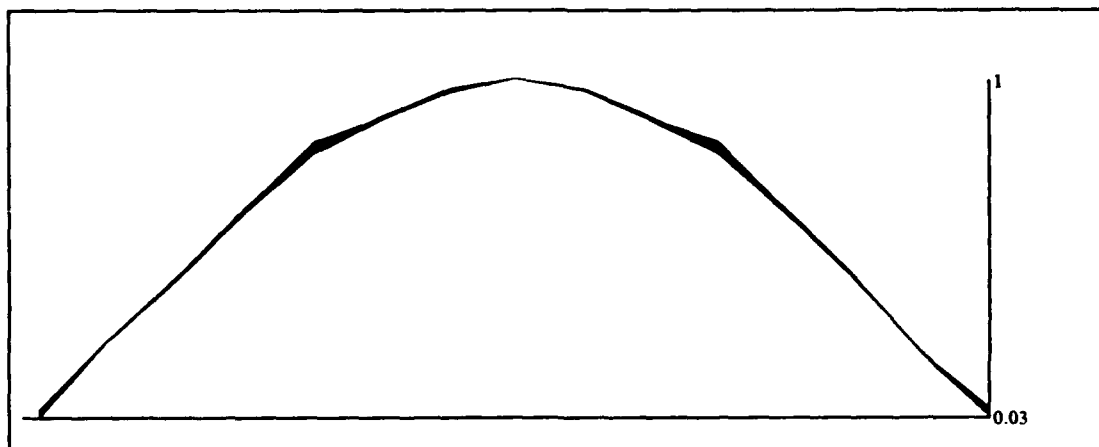
Comparison of Strain Gage to
Laser Interferometer Displacement Data
Flexdisk 42A
2.8 Volts

Strain Measurements taken at 24 Deg C
Displacement measurements taken at 24 Deg C

$A = READPRN(strain)$ **Reads Data from strain gages on transducers face**

Data is read into matrices of the form

	Frequency (Hz)	Voltage Level (dB)	Phase (Deg)

$R1 = 167$ $R2 = 267$ $I = R1, 168 .. R2$

Voltage levels are taken in dB, must be converted to volts

$$A_{1,1} = 10^{\frac{A_{1,1}}{20}}$$

Convert Strain RMS voltage to peak

$$A_{1,1} = \frac{A_{1,1} \cdot \sqrt{2}}{1000}$$

Convert Voltage to strain

Gage Factor $GF = 2.095$ $V = I \cdot \Omega$

$\Omega = 1400$

$i = .004$ $\Delta\Omega_1 = \frac{A_{1,1}}{i}$

$Strain_{1,1} = \frac{\Delta\Omega_1}{\Omega \cdot GF}$ $Strain_{1,0} = A_{1,0}$

Plot of Strain vs Frequency

$J = 0 .. 100$

$Str_{J,1} = Strain_{J+R1-1,1}$ $Str_{J,0} = Strain_{J+R1-1,0}$ $max(Strain^{<1>}) = 1.00360529 \cdot 10^{-6}$

Plot Maximum Displacement Vs Frequency for Comparison

$I = 0 .. 100$ $D = \text{READPRN}(D)$ $E_{1,1} = D_{1,7}$ $E_{1,0} = ((I + R1) \cdot 5) + 3000$

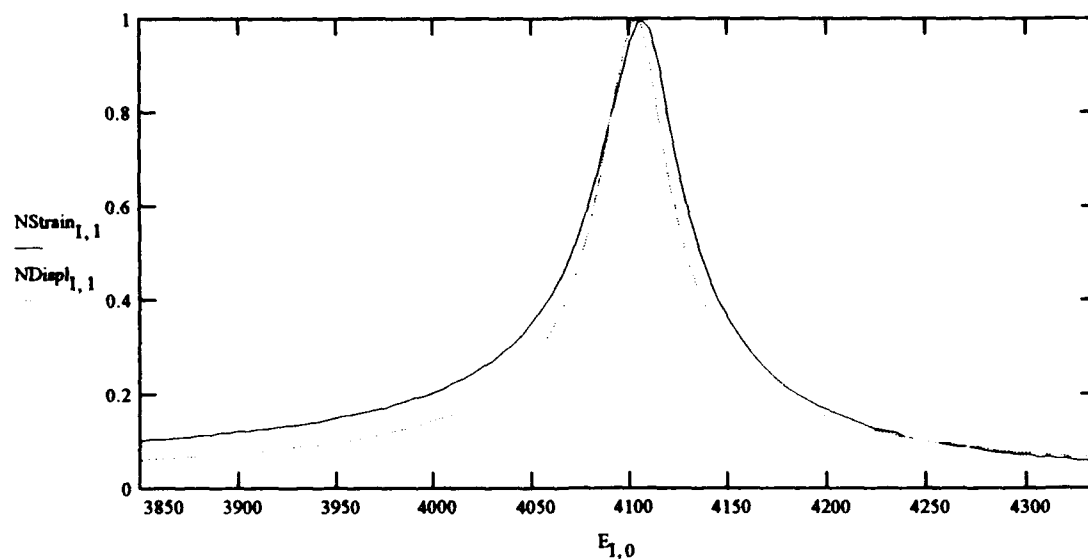## Plot of displacement of center focal point
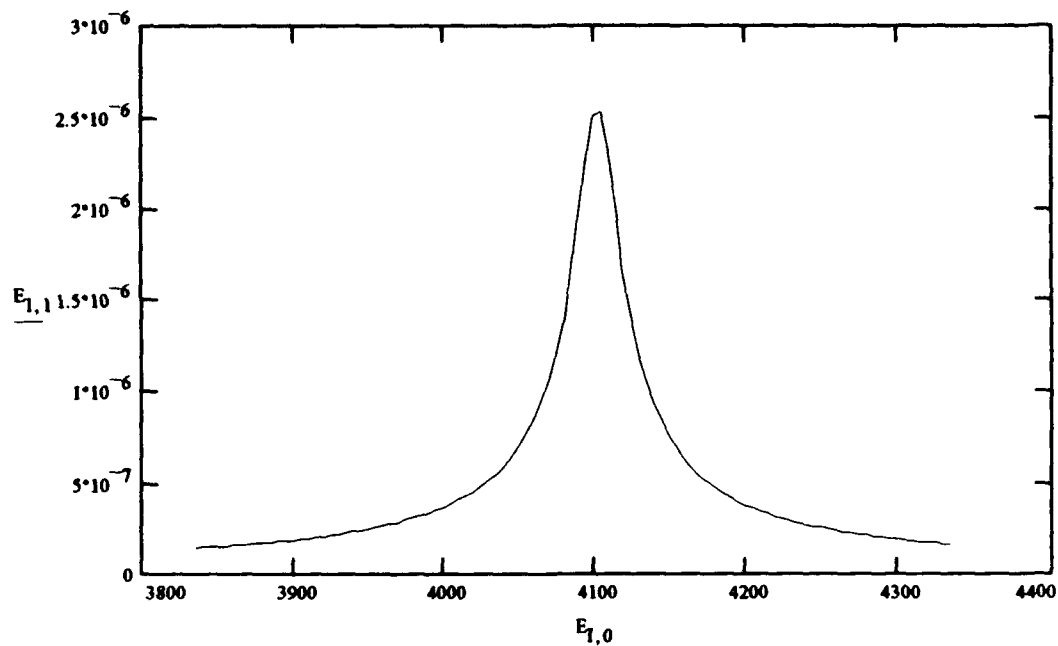
Write calculated strain data to file Strain and Maximum displacement (radius 0) to file MDispl

$\text{WRITEPRN}(\text{Strain}) = \text{Str}$ $\text{WRITEPRN}(\text{MDispl}) = E$

Plot Normalized Strain and displacement

$$\max\left(\text{Str}^{<1>}\right) = 1.00360529 \cdot 10^{-6} \quad \max\left(E^{<1>}\right) = 2.526 \cdot 10^{-6}$$

$$\text{NStrain}_{1,1} = \frac{\text{Str}_{1,1}}{\max\left(\text{Str}^{<1>}\right)} \qquad \text{NDispl}_{1,1} = \frac{E_{1,1}}{\max\left(E^{<1>}\right)}$$

APPENDIX C

This appendix contains the results of the experiments on flexural disk 42B. All of the calculations are performed using Mathcad and are discussed in the text.

Surface plots of displacement and phase of 42B

2.951·10^{-6}

5.508·10^{-9}

D

1.556

1.475

P
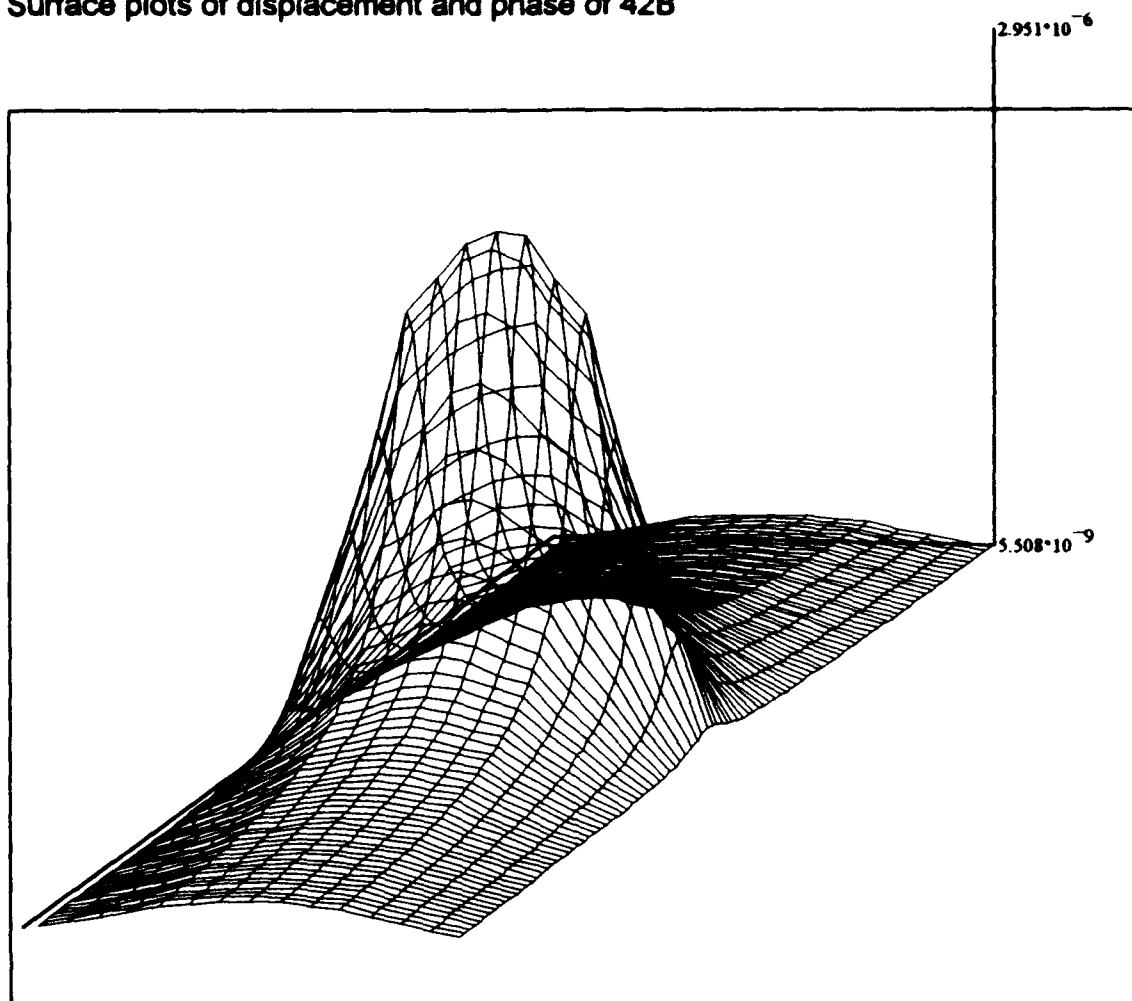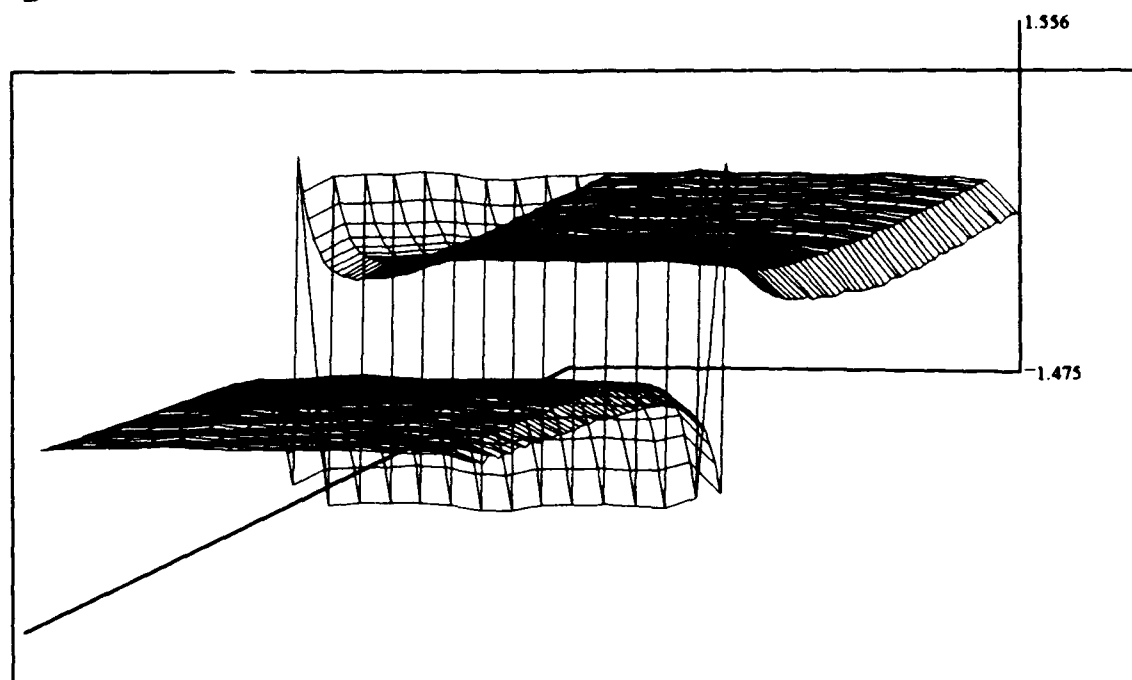
Normalization of Displacement Data

FD42B, 2.8 Volts

$D = READPRN(D)$
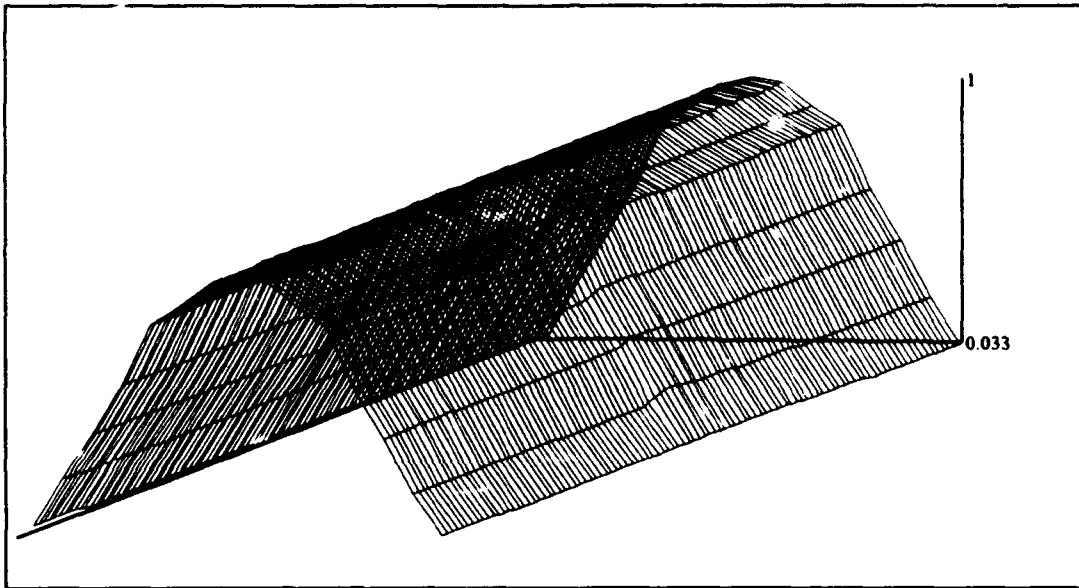
Normalize all data for each frequency to the max value

$rows(D) = 101 \qquad cols(D) = 15 \qquad max(D) = 2.951 \cdot 10^{-6}$

$J = 0..100 \qquad I = 0..14 \qquad M = max(D) \qquad M = 2.951 \cdot 10^{-6}$

$D = D^T$

$M_J = max\left(D^{<J>}\right) \qquad D_{I,J} = \dfrac{D_{I,J}}{M_J}$

$D = D^T \qquad Ndispl_{I,0} = \dfrac{I}{2} - 3.5 \qquad Ndispl_{I,1} = D_{I,7} \qquad WRITEPRN(NDispl) = Ndispl$

D

Viewing the same plot on end, 42B

D
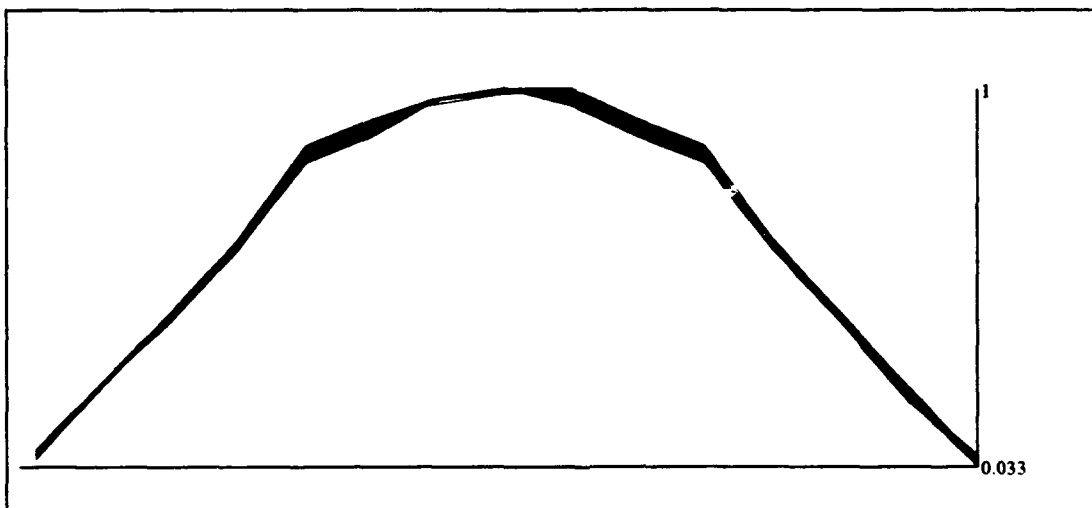
Comparison of Strain Gage to
Laser Interferometer Displacement Data

Flexdisk 42B
2.8 Volts

Strain Measurements taken at 24 Deg C

Displacement measurements taken at 24 Deg C

$A = \text{READPRN(strain)}$ Reads Data from strain gages on transducers face

Data is read into matrices of the form

Frequency (Hz)	Voltage Level (dB)	Phase (Deg)

$R1 = 167$ $R2 = 267$ $I = R1, 168..R2$

Voltage levels are taken in dB, must be converted to volts

$$A_{1,1} = 10^{\frac{A_{1,1}}{20}}$$

Convert Strain RMS voltage to peak

$$A_{1,1} = \frac{A_{1,1} \cdot \sqrt{2}}{1000}$$

Convert Voltage to strain

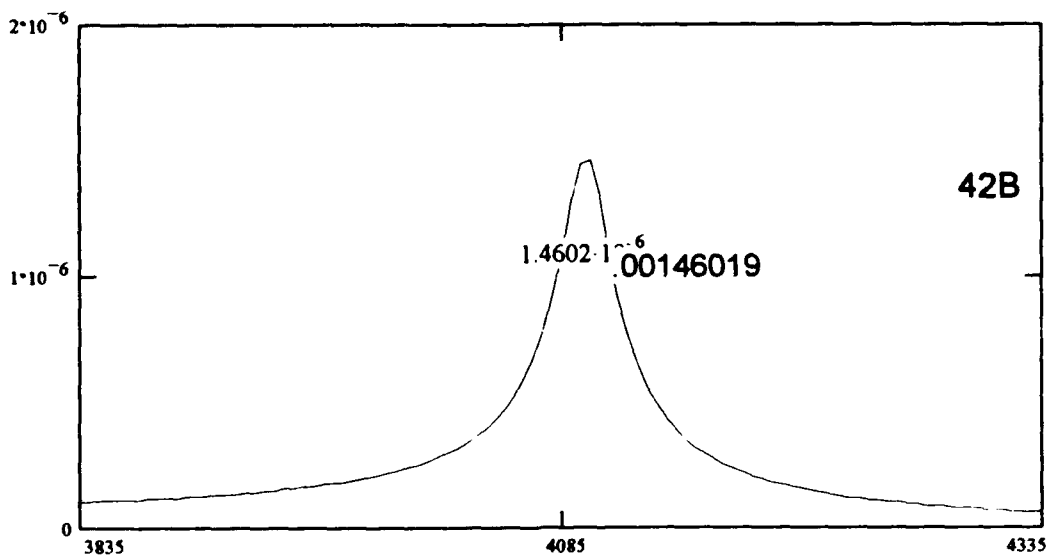Gage Factor $GF = 2.095$ $V = I \cdot \Omega$

$\Omega = 1400$

$i = .004$ $\Delta\Omega_I = \dfrac{A_{1,1}}{i}$

$$\text{Strain}_{1,1} = \frac{\Delta\Omega_I}{\Omega \cdot GF} \qquad \text{Strain}_{1,0} = A_{1,0}$$

Plot of Strain vs Frequency
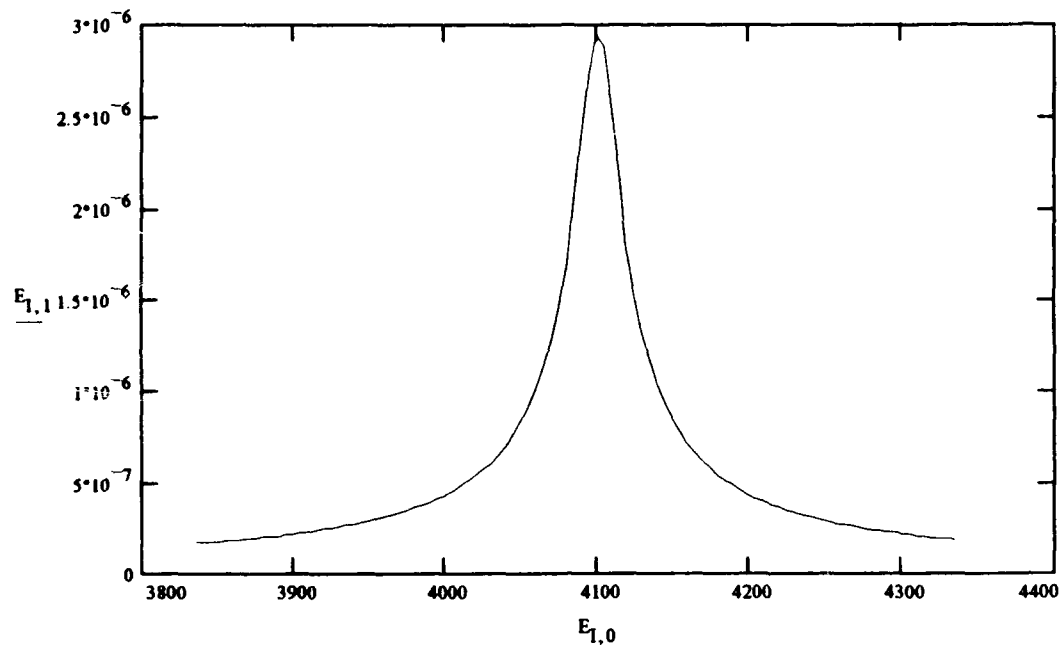

42B

1.4602·10⁻⁶ .00146019

$J = 0..100$

$$\text{Str}_{J,1} = \text{Strain}_{J+R1-1,1} \qquad \text{Str}_{J,0} = \text{Strain}_{J+R1-1,0}$$

$$\max\left(\text{Strain}^{<1>}\right) = 1.4602 \cdot 10^{-6}$$

62

Plot Maximum Displacement Vs Frequency for Comparison

$I = 0..100$ $\quad$ $D = READPRN(D)$ $\quad$ $E_{I,1} = D_{I,7}$ $\quad$ $E_{I,0} = ((1 + R1) \cdot 5) + 3000$

Plot of displacement of center focal point

Write calculated strain data to file Strain and Maximum displacement (radius 0) to file MDispl

$WRITEPRN(Strain) = Str$ $\qquad$ $WRITEPRN(MDispl) = E$

Plot Normalized Strain and displacement

$$\max\left(Str^{<1>}\right) = 1.4602 \cdot 10^{-6} \qquad \max\left(E^{<1>}\right) = 2.951 \cdot 10^{-6}$$

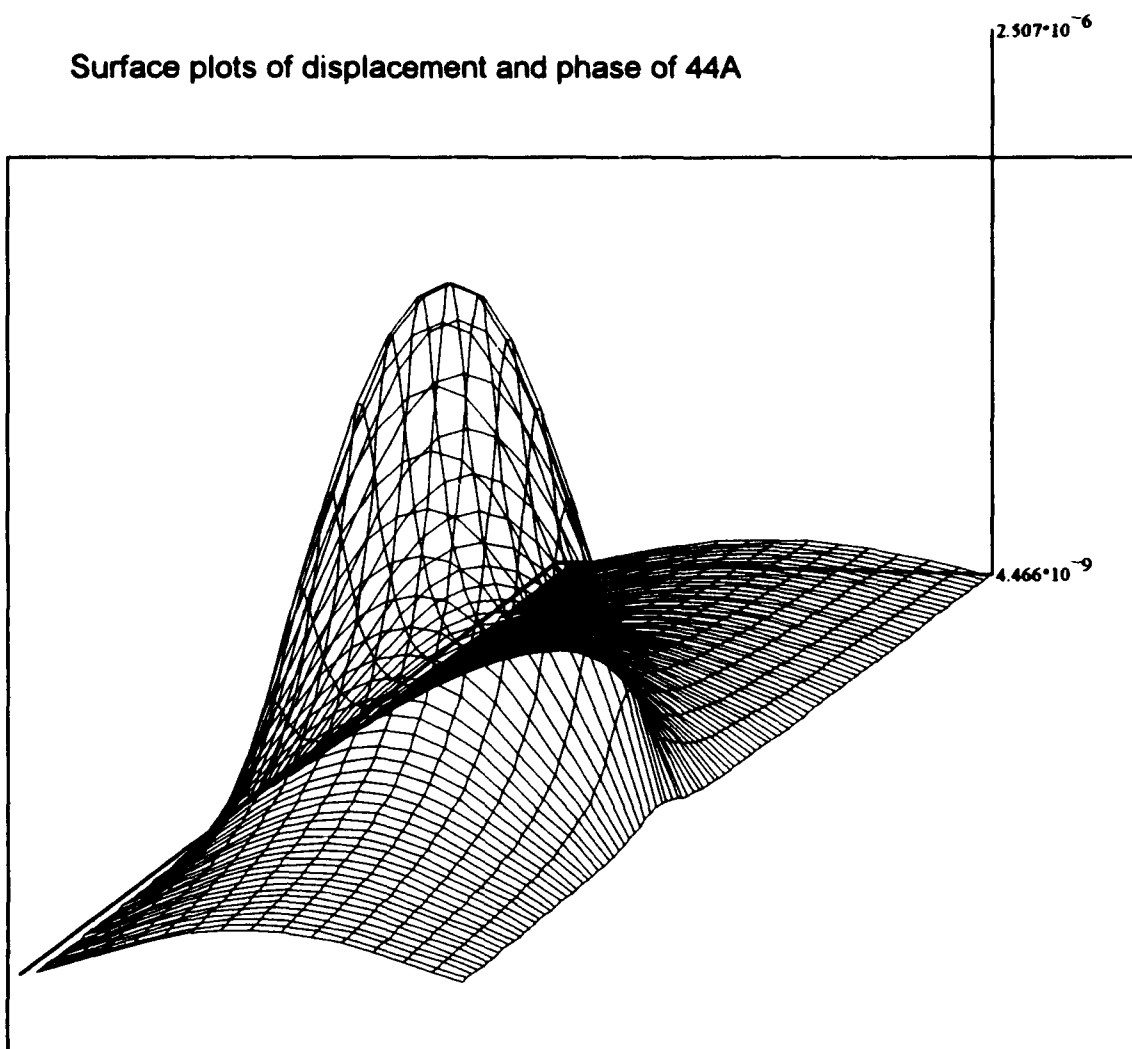$$NStrain_{I,1} = \frac{Str_{I,1}}{\max\left(Str^{<1>}\right)} \qquad NDispl_{I,1} = \frac{E_{I,1}}{\max\left(E^{<1>}\right)}$$
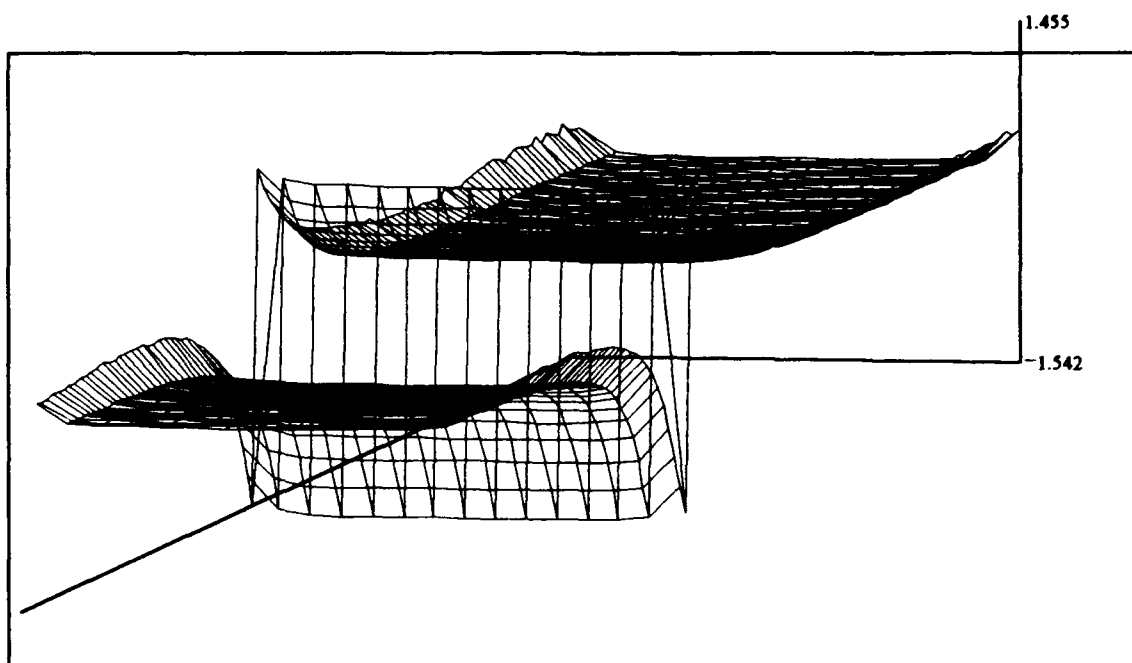

63

APPENDIX D

This appendix contains the results of the experiments on flexural disk 44A. All of the calculations are performed using Mathcad and are discussed in the text.

Surface plots of displacement and phase of 44A

D

P

Normalization of Displacement Data

FD44A, 2.8 Volts

$D := READPRN(D)$

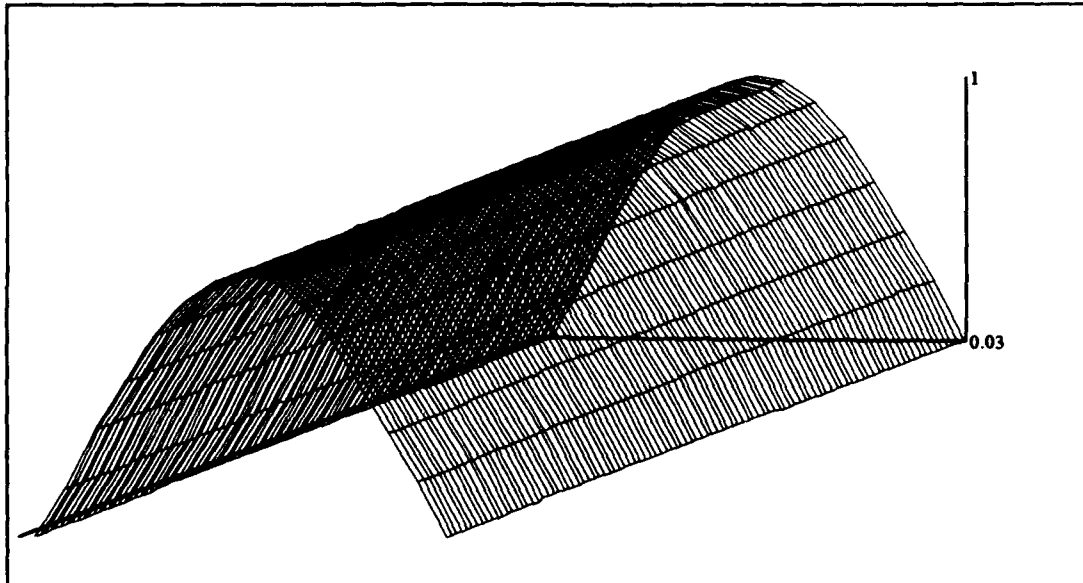## Normalize all data for each frequency to the max value

$rows(D) = 101$ $\qquad cols(D) = 15$ $\qquad max(D) = 2.507 \cdot 10^{-6}$

$J := 0..100$ $\qquad I := 0..14$ $\qquad M := max(D)$ $\qquad M = 2.507 \cdot 10^{-6}$

$D := D^T$

$M_J = max(D^{<J>})$ $\qquad D_{I,J} := \dfrac{D_{I,J}}{M_J}$

$\qquad\qquad Ndispl_{I,0} := \dfrac{I}{2} - 3.5$ $\qquad Ndispl_{I,1} := D_{I,7}$ $\quad WRITEPRN(NDispl) := Ndispl$

$D := D^T$

D

Viewing the same plot of 44A on end
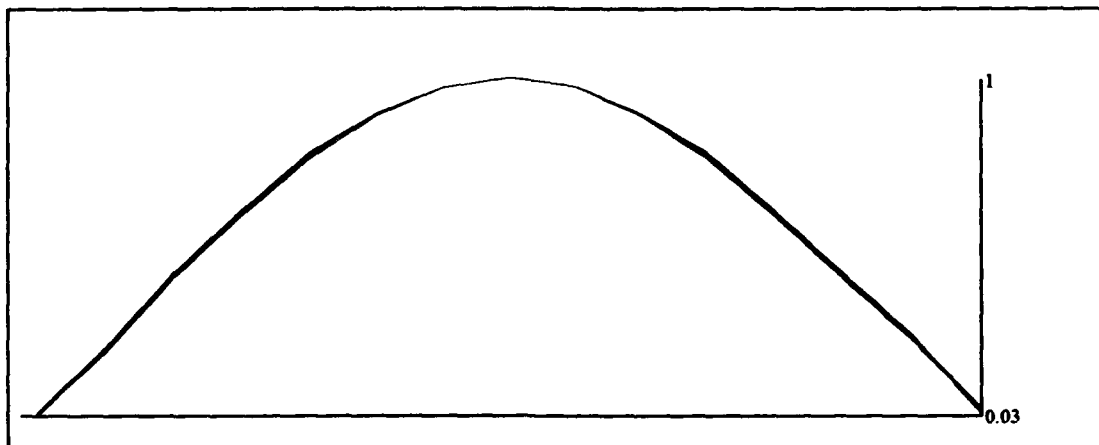
D

Comarison of Strain Gage to
Laser Interferometer Displacement Data
Flexdisk 44A
2.8 Volts

Strain Measurements taken at 24 Deg C

Displacement measurements taken at 24 Deg C

A = READPRN(strain)   Reads Data from strain gages on transducers face

Data is read into matrices of the form

	Frequency (hz)		Voltage Level (dB)		Phase (Deg)
R1 = 167	R2 = 267	I = R1, 168..R2			

Voltage levels are taken in dB, must be converted to volts

$$A_{I,1} = 10^{\frac{A_{I,1}}{20}}$$

Convert Strain RMS voltage to peak

$$A_{I,1} = \frac{A_{I,1} \cdot \sqrt{2}}{1000}$$

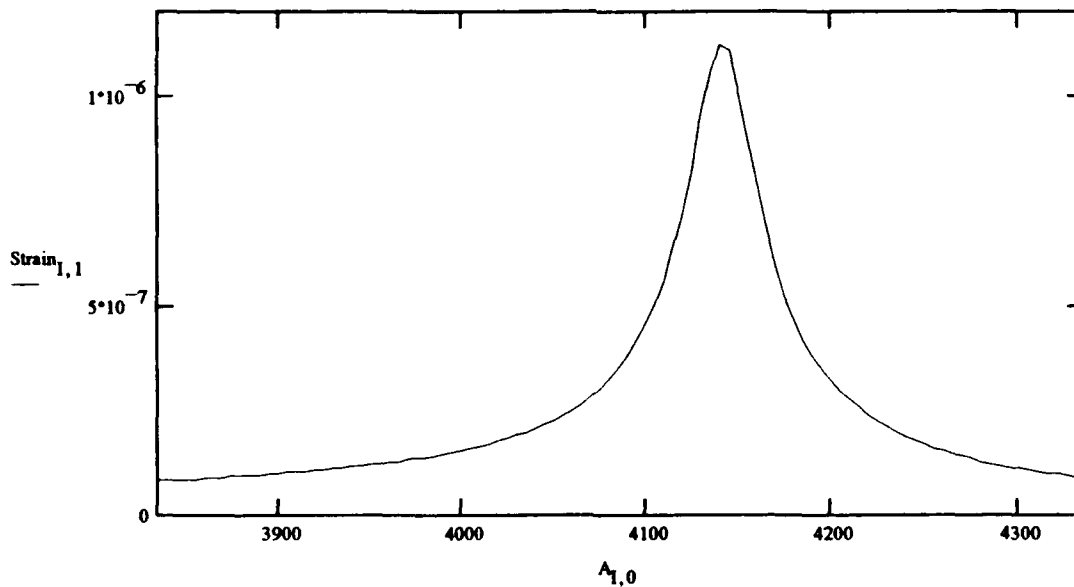Convert Voltage to strain

Gage Factor $GF = 2.095$ $V = I \cdot \Omega$

$\Omega = 1400$

$i = .004$ $\Delta\Omega_I = \frac{A_{I,1}}{i}$

$Strain_{I,1} = \frac{\Delta\Omega_I}{\Omega \cdot GF}$ $Strain_{I,0} = A_{I,0}$

Plot of Strain vs Frequency

$J = 0..100$ — trace 1

$Str_{J,1} = Strain_{J+R1-1,1}$ $Str_{J,0} = Strain_{J+R1-1,0}$ $max(Strain^{<1>}) = 1.12 \cdot 10^{-6}$

Plot Maximum Displacement Vs Frequency for Comparison

$I = 0..100$ $\quad$ $D = READPRN(D)$ $\quad$ $E_{I,1} = D_{I,7}$ $\quad$ $E_{I,0} = ((I + R1) \cdot 5) + 3000$

Plot of displacement of center focal point
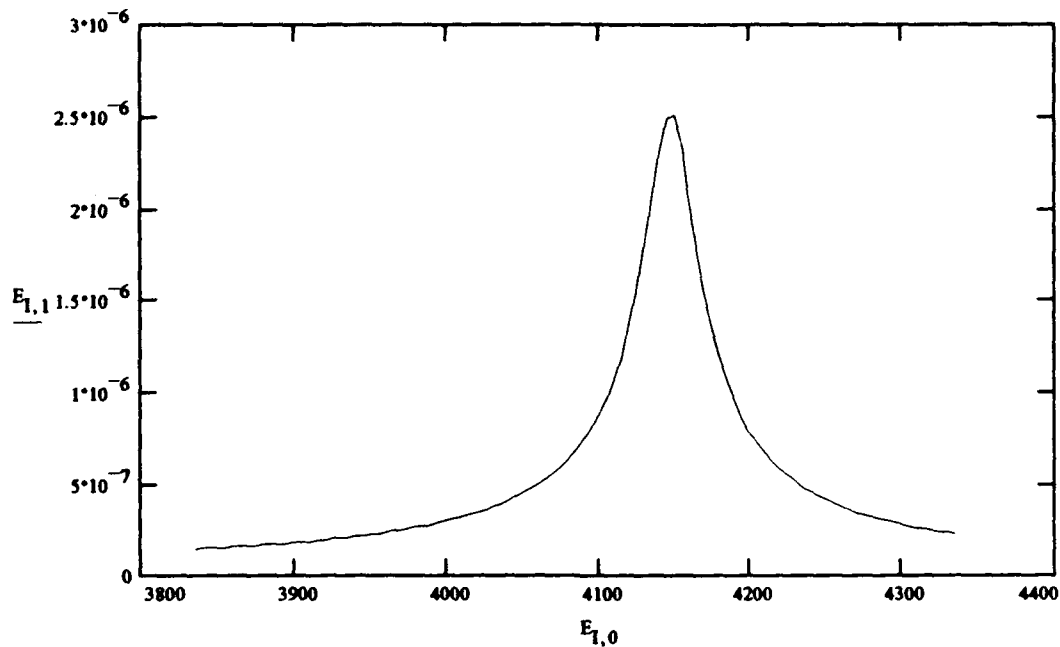
Write calculated strain data to file Strain and Maximum displacement (radius 0) to file MDispl

$WRITEPRN(Strain) = Str$ $\qquad$ $WRITEPRN(MDispl) = E$

Plot Normalized Strain and displacement

$$\max\left(Str^{<1>}\right) = 1.12 \cdot 10^{-6} \qquad\qquad \max\left(E^{<1>}\right) = 2.507 \cdot 10^{-6}$$

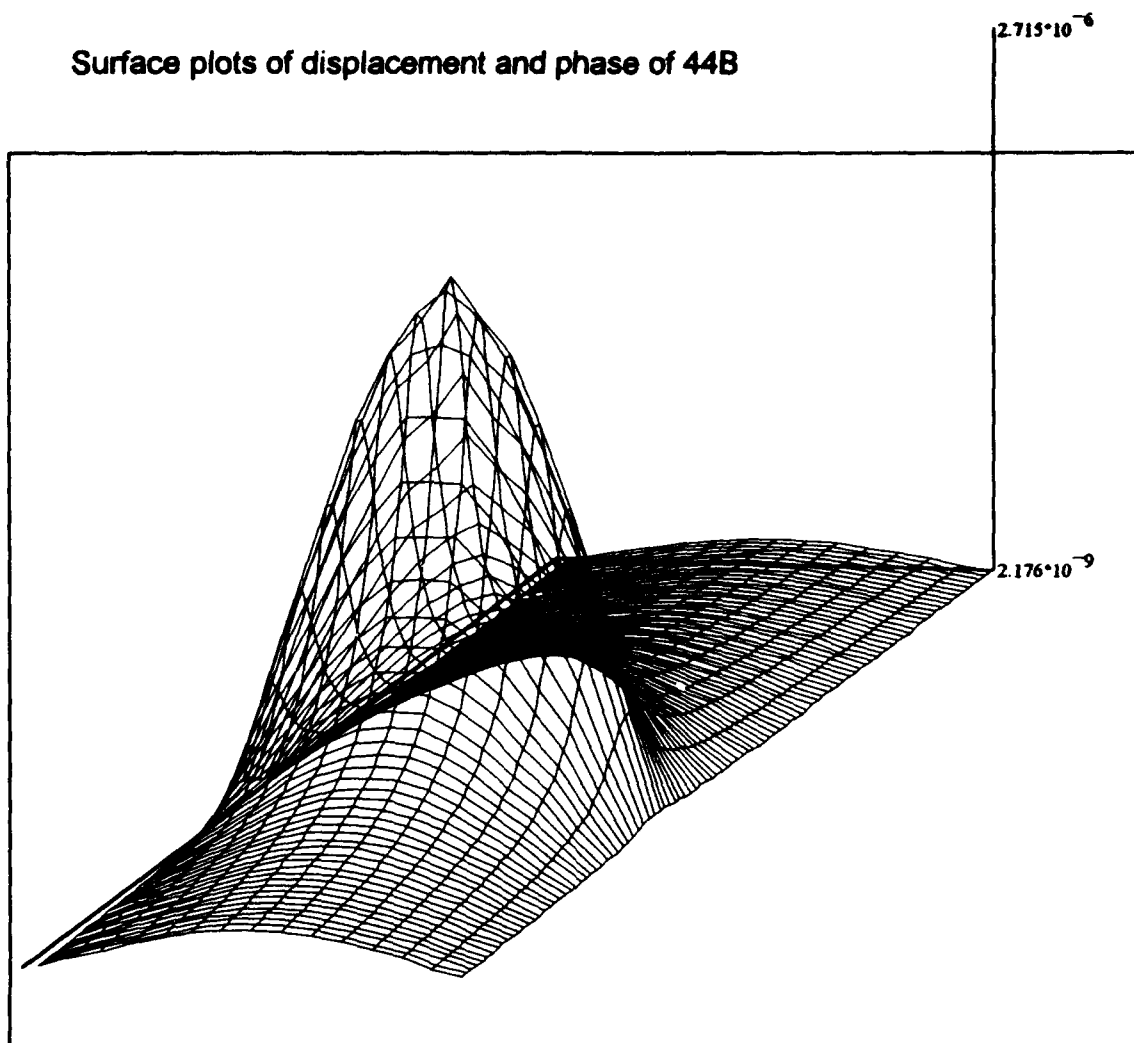$$NStrain_{I,1} = \frac{Str_{I,1}}{\max\left(Str^{<1>}\right)} \qquad\qquad NDispl_{I,1} = \frac{E_{I,1}}{\max\left(E^{<1>}\right)}$$
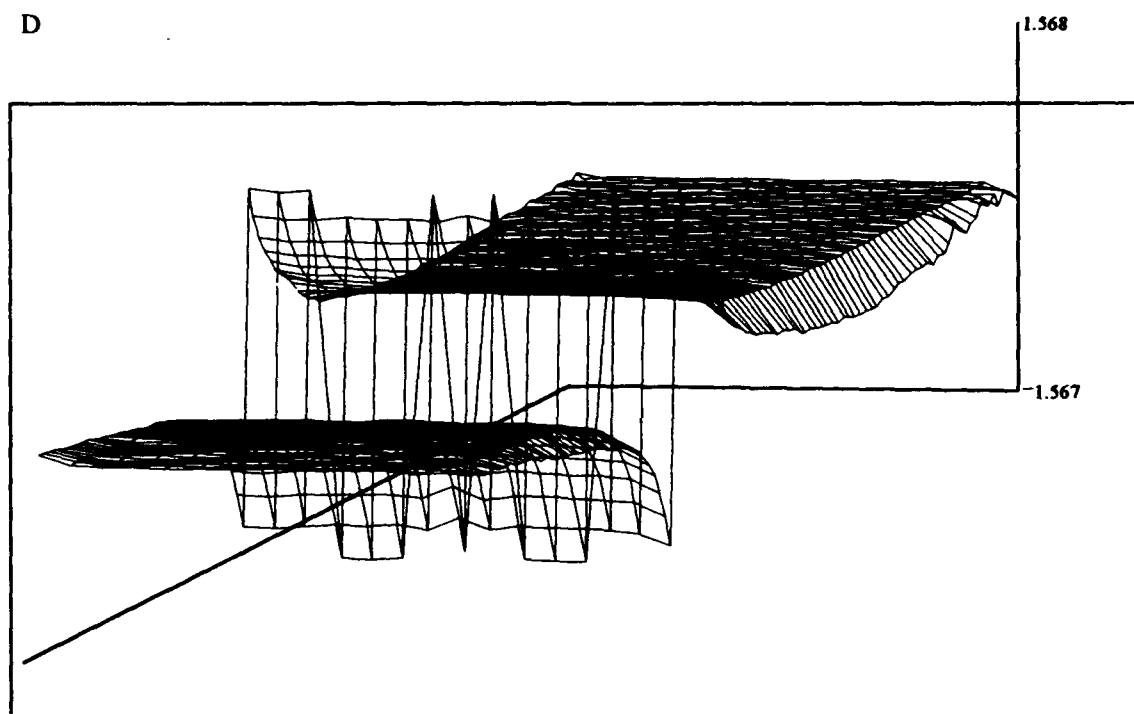
APPENDIX E

This appendix contains the results of the experiments on flexural disk 44B. All of the calculations are performed using Mathcad and are discussed in the text.

Surface plots of displacement and phase of 44B

D

P

Normalization of Displacement Data

FD44B, 2.8 Volts

$D = \text{READPRN}(D)$
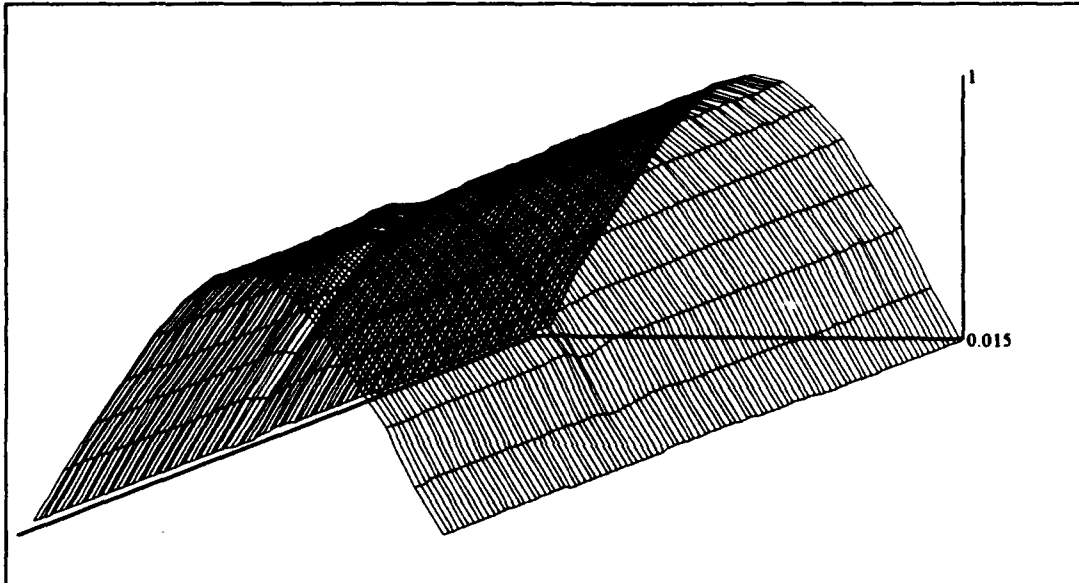
Normalize all data for each frequency to the max value

$\text{rows}(D) = 101 \qquad \text{cols}(D) = 15 \qquad \max(D) = 2.715 \cdot 10^{-6}$

$J = 0 .. 100 \qquad I = 0 .. 14 \qquad M = \max(D) \qquad M = 2.715 \cdot 10^{-6}$

$D = D^T$

$M_J = \max\left(D^{\langle J \rangle}\right) \qquad D_{I,J} = \dfrac{D_{I,J}}{M_J}$

$D = D^T \qquad \text{Ndispl}_{I,0} = \dfrac{I}{2} - 3.5 \qquad \text{Ndispl}_{I,1} = D_{I,7} \qquad \text{WRITEPRN}(\text{NDispl}) = \text{Ndispl}$

D

Viewing the same plot on end

D
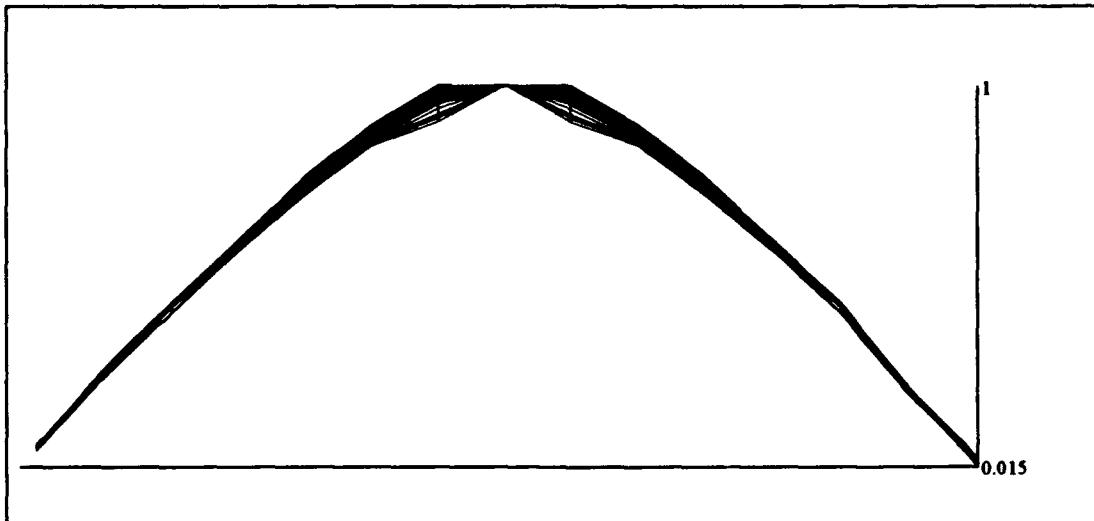
Comparison of Strain Gage to
Laser Interferometer Displacement Data
Flexdisk 44B
2.8 Volts

Strain Measurements taken at 24 Deg C

Displacement measurements taken at 24 Deg C

A = READPRN(strain)   Reads Data from strain gages on transducers face

Data is read into matrices of the form

| Frequency (Hz) | Voltage Level (dB) | Phase (Deg) |

$R1 = 167$ $R2 = 267$ $I = R1, 168 .. R2$

Voltage levels are taken in dB, must be converted to volts

$$A_{1,1} = 10^{\frac{A_{1,1}}{20}}$$

Convert Strain RMS voltage to peak

$$A_{1,1} = \frac{A_{1,1} \cdot \sqrt{2}}{1000}$$

Convert Voltage to strain

Gage Factor $GF = 2.095$ $V = I \cdot \Omega$

$\Omega = 1400$
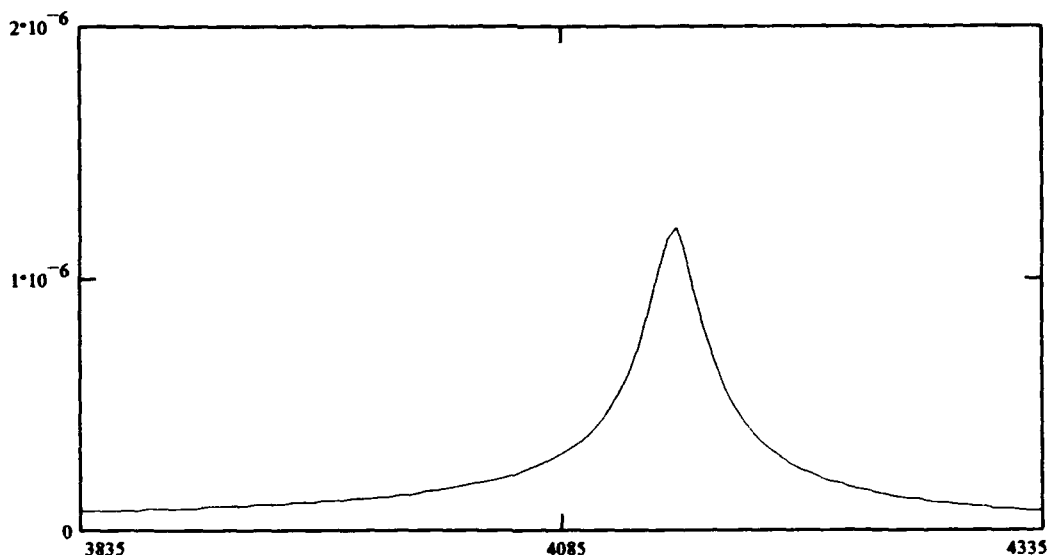
$i = .004$ $\Delta\Omega_1 = \frac{A_{1,1}}{i}$

$Strain_{1,1} = \frac{\Delta\Omega_1}{\Omega \cdot GF}$ $Strain_{1,0} = A_{1,0}$

Plot of Strain vs Frequency

$J = 0 .. 100$
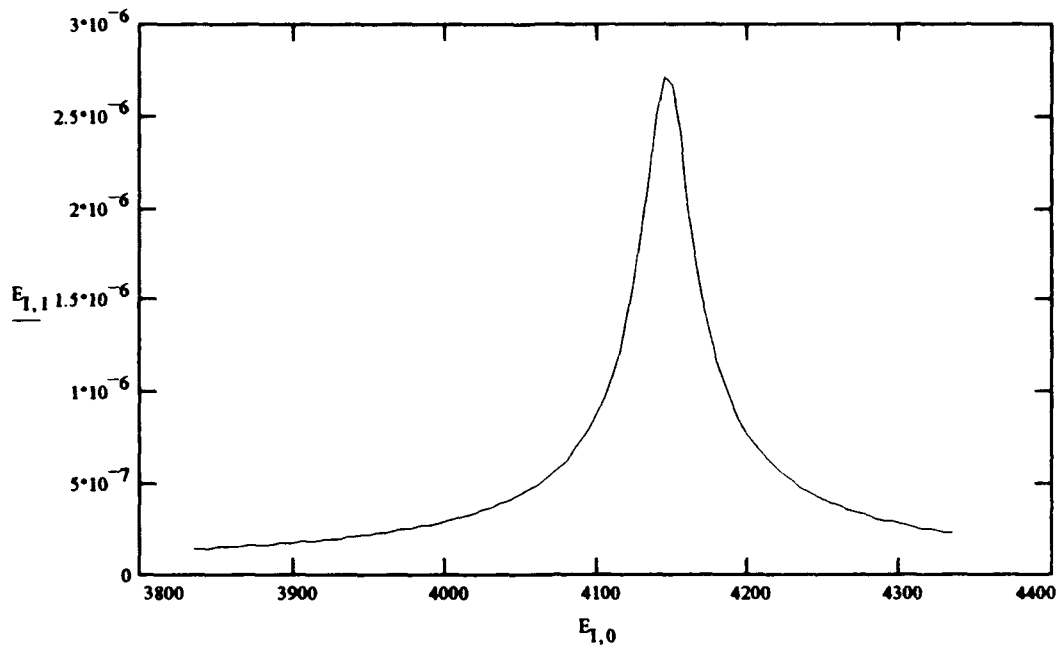
$Str_{J,1} = Strain_{J+R1-1,1}$ $Str_{J,0} = Strain_{J+R1-1,0}$ $\max\left(Strain^{<1>}\right) = 1.205 \cdot 10^{-6}$

Plot Maximum Displacement Vs Frequency for Comparison (44B)

$I = 0 .. 100$ $D = READPRN(D)$ $E_{I,1} = D_{I,7}$ $E_{I,0} = ((I + RI) \cdot 5) + 3000$

Plot of displacement of center focal point

$E_{I,1}$

3850   3900   3950   4000   4050   4100   4150   4200   4250   4300

$E_{I,0}$

Write calculated strain data to file Strain and Maximum displacement (radius 0) to file MDispl

$WRITEPRN(Strain) = Str$ $WRITEPRN(MDispl) = E$

Plot Normalized Strain and displacement

$max\left(Str^{<1>}\right) = 1.205 \cdot 10^{-6}$ $max\left(E^{<1>}\right) = 2.715 \cdot 10^{-6}$

$$NStrain_{I,1} = \frac{Str_{I,1}}{max\left(Str^{<1>}\right)}$$ $$NDispl_{I,1} = \frac{E_{I,1}}{max\left(E^{<1>}\right)}$$

$NStrain_{I,1}$

$NDispl_{I,1}$

3850   3900   3950   4000   4050   4100   4150   4200   4250   4300

$E_{I,0}$

73

LIST OF REFERENCES

1. Woollett, R.S., <u>Theory of Piezoelectric Flexural Disk Transducer With Applications to Underwater Sound</u>, U.S. Navy Underwater Sound Laboratory, New London, Connecticut, 1960.

2. Lindberg, J.F., <u>Design Considerations for a Liquid Backed Tri-laminar Flexural Disk Transducer for use in a Torpedo Conformal Array</u>, Naval Underwater Systems Center, Newport Rhode Island, 1981.

3. Wilson O.B., <u>Introduction to Theory and Design of Sonar Transducers</u>, Peninsula Publishing, Los Altos California, 1988.

4. Polytec, <u>VIB-MAN-9107-e01 Polytec OVF 350 Operating Manual.</u>

5. O'Shea D.C., Callen R.W., Rhodes W.T., <u>Introduction to Lasers and Their Applications</u>, Addison-Wesley Publishing Company, Reading, Massachusetts, 1978.

6. Measurements Group, <u>Catalogue 500</u>, Raleigh, North Carolina, 1988.

7. Mathsoft Inc., <u>Mathcad 3.0 Users Guide</u>, Cambridge Massachusets, 1991.

8. Kinsler, Frey, Coppens, Sanders, <u>Fundamentals of Acoustics</u>, John Wiley & Sons, New York, New York, 1982.

INITIAL DISTRIBUTION LIST

1. Defense Technical Information Center   2
   Cameron Station
   Alexandria, Virginia   22304-6145

2. Library, Code 52   2
   Naval Postgraduate School
   Monterey, California   93943-5002

3. Professor Anthony A. Atchley, Code PH/Ay   1
   Department of Physics
   Naval Postgraduate School
   Monterey, California   93943-5000

4. Professor Steven R. Baker, Code PH/Ba   2
   Department of Physics
   Naval Postgraduate School
   Monterey, California   93943-5000

5. Professor Oscar B. Wilson, Code PH/Wl   1
   Department of Physics
   Naval Postgraduate School
   Monterey, California   93943-5000

6. Mr. Ed Rynne, Code 711   1
   Naval Command, Control and Ocean Surveillance Center
   Research, Development, Test and Evaluation Division
   San Diego, California   92152-5000

7. Mr. Roger Richards, Code 213   1
   Naval Undersea Warfare Center
   New London, Connecticut   06320

8. Mr. Robert Timme   1
   Naval Research Lab-USRD
   Orlando, Florida   32856

9. Mr. Cliff Meland, Code 712   1
   75Naval Command, Control and Ocean Surveillance Center
   Research, Development, Test and Evaluation Division
   San Diego, California   92152-5000

10 Mr. Bernard F. Hamonic   1
   Institut Superieur d'Electronique du Nord
   41 Blvd Vauban
   59046 Lille, Cedex, France